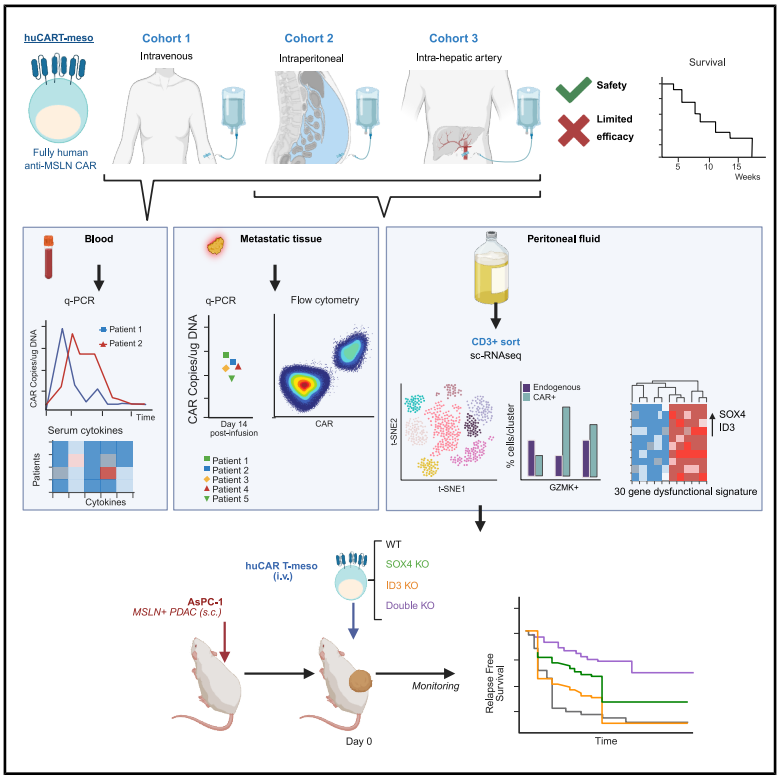
Cell Reports
Medicine

Article

Clinical and molecular dissection of CAR T cell resistance in pancreatic cancer

Graphical abstract



Highlights

- Anti-mesothelin CAR T therapy is well tolerated in advanced PDAC but shows limited efficacy
- Transcriptomic analyses reveal that patient CAR T cells are dysfunctional
- ID3 and SOX4 double-knockout CAR T cells elicited prolonged relapse-free survival *in vivo*

Authors

M. Angela Aznar, Charly R. Good, Julie S. Barber-Rotenberg, ..., Shelley L. Berger, Carl H. June, Mark H. O'Hara

Correspondence

ryoung@upenn.edu (R.M.Y.), bergers@pennmedicine.upenn.edu (S.L.B.), cjune@upenn.edu (C.H.J.), mark.ohara@pennmedicine.upenn.edu (M.H.O.)

In brief

Aznar and Good et al. report a phase 1 trial of anti-mesothelin CAR T cells in pancreatic cancer, demonstrating safety but limited efficacy. Locally delivered CAR T cells exhibit GZMK^{+} phenotypes and a dysfunctional signature including ID3 and SOX4 upregulation. Dual-knockout CAR T cells elicit prolonged relapse-free survival *in vivo*.

Aznar et al., 2025, Cell Reports Medicine *6*, 102301
September 16, 2025 © 2025 The Authors. Published by Elsevier Inc.
https://doi.org/10.1016/j.xcrm.2025.102301

CellPress

Cell Reports Medicine

CellPress
OPEN ACCESS

Article

Clinical and molecular dissection of CAR T cell resistance in pancreatic cancer

M. Angela Aznar,[1,2,17] Charly R. Good,[3,17] Julie S. Barber-Rotenberg,[1] Sangya Agarwal,[1,15] Wesley Wilson,[1] Alex Watts,[4] Zhen Zhang,[3] Donna Gonzales,[1] Greg Donahue,[3] Wei-Ting Hwang,[4] Austin K. Rennels,[1] Andrew J. Rech,[1] Shunichiro Kuramitsu,[1,16] Hua Huang,[3,13,14] Karl M. Glastad,[3] Katherine A. Alexander,[3] Gabriela Plesa,[1] Emily Dowd,[1] Andrea Brennan,[1] Donald L. Siegel,[1,2] Janos Tanyi,[5,6] Andrew Haas,[5,7] Drew A. Torigian,[5,8] Gregory Nadolski,[5,8] Vanessa E. Gonzalez,[1] Elizabeth O. Hexner,[1,9] Joseph A. Fraietta,[1,2,5,10] Julie K. Jadlowsky,[1] Regina M. Young,[1,2,11,18,*] Shelley L. Berger,[3,18,*] Carl H. June,[1,2,11,18,19,*] and Mark H. O'Hara[5,12,18,*]

[1]Center for Cellular Immunotherapies, University of Pennsylvania Perelman School of Medicine, Philadelphia, PA 19104, USA
[2]Department of Pathology and Laboratory Medicine, University of Pennsylvania Perelman School of Medicine, Philadelphia, PA 19104, USA
[3]Department of Cell and Developmental Biology, Penn Epigenetics Institute, Perelman School of Medicine, Philadelphia, PA 19104, USA
[4]Department of Biostatistics, Epidemiology and Informatics, Perelman School of Medicine, University of Pennsylvania, Philadelphia, PA 19104, USA
[5]Abramson Cancer Center, University of Pennsylvania, Philadelphia, PA 19104, USA
[6]Ovarian Cancer Research Center, Perelman School of Medicine, University of Pennsylvania, Philadelphia, PA 19104, USA
[7]Division of Pulmonary, Allergy, and Critical Care, Department of Medicine, Perelman School of Medicine, University of Pennsylvania, Philadelphia, PA 19104, USA
[8]Department of Radiology, Perelman School of Medicine, University of Pennsylvania, Philadelphia, PA, USA
[9]Division of Hematology/Oncology, Department of Medicine, University of Pennsylvania Perelman School of Medicine, Philadelphia, PA 19104, USA
[10]Department of Microbiology, Perelman School of Medicine, University of Pennsylvania, Philadelphia, PA 19104, USA
[11]Parker Institute for Cancer Immunotherapy, University of Pennsylvania, Philadelphia, PA 19104, USA
[12]Department of Medicine, Division of Hematology and Oncology, Perelman School of Medicine, University of Pennsylvania, Philadelphia, PA 19104, USA
[13]Department of Systems Pharmacology and Translational Therapeutics, University of Pennsylvania Perelman School of Medicine, Philadelphia, PA 19104, USA
[14]Institute for Immunology and Immune Health, University of Pennsylvania Perelman School of Medicine, Philadelphia, PA 19104, USA
[15]Present address: Center for Personal Dynamic Regulomes, Stanford University School of Medicine, Stanford, CA 94305, USA
[16]Present address: Department of Neurosurgery, National Hospital Organization Nagoya Medical Center, Nagoya 460-0001, Japan
[17]These authors contributed equally
[18]These authors contributed equally
[19]Lead contact
*Correspondence: ryoung@upenn.edu (R.M.Y.), bergers@pennmedicine.upenn.edu (S.L.B.), cjune@upenn.edu (C.H.J.), mark.ohara@pennmedicine.upenn.edu (M.H.O.)
https://doi.org/10.1016/j.xcrm.2025.102301

SUMMARY

Patients with advanced pancreatic ductal adenocarcinoma (PDAC) have a median survival of less than a year, highlighting the urgent need for treatment advancements. We report on a phase 1 clinical trial assessing the safety and feasibility of intravenous and local administration of anti-mesothelin CAR T cells in patients with advanced PDAC. While therapy is well tolerated, it demonstrates limited clinical efficacy. Analyses of patient samples provide insights into mechanisms of treatment resistance. Single-cell genomic approaches reveal that post-infusion CAR T cells express exhaustion signatures, including previously identified transcription factors ID3 and SOX4, and display enrichment for a GZMK$^+$ phenotype. Single knockout of ID3 or SOX4 enhances efficacy in xenograft models, though with donor-dependent variability. However, single-knockout cells eventually fail. Conversely, ID3 and SOX4 double-knockout CAR T cells exhibit prolonged relapse-free survival, demonstrating a sustained therapeutic effect and a potential avenue for engineering more potent CAR T cells in PDAC. This study was registered at ClinicalTrials.gov (NCT03323944).

INTRODUCTION

Combination chemotherapy is the standard of care for metastatic pancreatic ductal adenocarcinoma (PDAC), but the overall benefit is marginal, and PDAC remains one of the most lethal malignancies.[1–3] Furthermore, despite the success of immune checkpoint blockade[4–6] and chimeric antigen receptor (CAR) T cell therapy[7,8] in various other cancers, their efficacy in

This is an open access article under the CC BY-NC license (http://creativecommons.org/licenses/by-nc/4.0/).

PDAC remains limited. Mesothelin (MSLN) is an attractive target for CAR T cell therapies for solid tumors given its overexpression in numerous cancers, including PDAC.[9–12] Moreover, elevated MSLN levels correlate with a worse prognosis in patients with PDAC[10,13] and are implicated in tumor progression.[14,15]

Our group has performed several phase 1 clinical trials evaluating MSLN-directed CAR T cells. First, we treated patients with chemotherapy-refractory metastatic PDAC with T lymphocytes electroporated with the murine anti-human MSLN ScFv SS-1 mRNA. This yielded a transient expression of the CAR and was associated with stable disease as the best response in two of five patients treated.[16] A follow-up study evaluated the stably transduced SS-1-based CAR in patients with malignant pleural mesothelioma, ovarian carcinoma, and PDAC (ClinicalTrials.gov: NCT02159716). While this treatment was tolerated, there was limited efficacy as the best response was stable disease in 11 out of 15 patients, including two out of five patients with PDAC.[17] In the phase 1 clinical trial described here, we evaluated a fully human anti-MSLN CAR construct (huCART-meso) in patients with histologically confirmed metastatic PDAC.

Current challenges limiting the efficacy of CAR T cell therapy for solid tumors include a hostile tumor microenvironment (TME), tumor heterogeneity, poor CAR T cell trafficking, T cell exhaustion and persistence, and the need for robust tumor-specific targets.[18] Chronic antigen exposure or a suppressive TME leads to exhaustion characterized by dysfunction of effector responses, sustained co-inhibitory receptor expression, and reprogrammed transcriptional and epigenetic states.[19–21] This dysfunction contributes to negative feedback mechanisms of T cell activation,[22] ultimately leading to diminished function.[23] Likewise, CAR T cells are susceptible to exhaustion following prolonged stimulation within the TME, thereby limiting their function.[24–26] In this regard, CD19 CAR T cells have demonstrated exhaustion phenotypes in patients with chronic lymphocytic leukemia and B cell lymphomas that do not respond to therapy.[24,27]

Developing synthetically enhanced CAR T cell therapies for solid tumors offers a promising strategy to overcome CAR T cell dysfunction.[28] Targeting transcription factors that regulate exhaustion has shown efficacy in reducing T cell receptor and CAR T cell exhaustion *in vitro* and in preclinical models.[26,29–31] In our previous work, we developed an *in vitro* model to generate exhausted MSLN-directed CAR T cells and showed that knocking out the transcriptional regulators inhibitor of DNA binding 3 (ID3) or SRY-box transcription factor 4 (SOX4) in CAR T cells increased their effector function upon chronic stimulation *in vitro*.[26]

Here, we report the clinical results of a phase 1 study of huCART-meso cells in patients with metastatic PDAC. To better understand responses, we report correlative analyses of blood, ascites fluid, and paired pre- and post-treatment biopsies of assessable metastases. We coupled these results with *in vivo* mouse models using ID3 and SOX4 knockout (KO) CAR T cells and high-throughput genomics experiments to provide insight into mechanisms of resistance to CAR T cell therapy for the treatment of patients with PDAC. We found that double KO of ID3 and SOX4 in CAR T cells improves long-term relapse-free survival *in vivo*, suggesting a potential therapeutic strategy.

RESULTS

Efficacy of huCART-meso cell therapy is limited

This was a phase 1, single-institution trial (ClinicalTrials.gov: NCT03323944) to evaluate the safety and feasibility of both intravenous (i.v.) administration and local delivery of lentiviral-transduced huCART-meso cells in patients with histologically confirmed unresectable or metastatic PDAC who had received at least 1 prior line of systemic chemotherapy. Patients received $1–3 \times 10^7/m^2$ huCART-meso cells via i.v. infusion (cohort 1), and the protocol was subsequently amended to include intraperitoneal (i.p.) (cohort 2) or intrahepatic (i.h.) delivery (via hepatic arterial infusion) (cohort 3). Patients infused on cohorts 2 and 3 were also eligible for up to two additional infusions of huCART-meso cells via i.v. administration at the same dose level, given between 21 and 42 days apart (Figure 1A). Three patients were infused in cohort 1, two patients were infused in cohort 2, and four patients were infused in cohort 3. Clinical and disease characteristics for the 9 patients infused with huCART-meso cells are listed in Table S1. The median age at study entry was 61 years (minimum 45 years to maximum 74 years) with three male (33.3%) and six female (66.7%) patients. All infused subjects were Caucasian. All patients (100%) previously received chemotherapy, while 2 (22.2%) were treated with surgery, 2 (22.2%) received targeted therapy, 2 (22.2%) received radiation therapy, and 1 (11.1%) received immunotherapy.

All patients received the protocol-specified dose of huCART-meso cells. All adverse events are summarized in Table 1. In cohort 1, we observed pulmonary toxicity in patients with moderate pulmonary metastatic burden, thought to be in part related to a first pass effect as we have published previously.[32] To mitigate this first pass effect and potentially enhance trafficking, we shifted to regional delivery for cohorts 2 and 3. Cytokine release syndrome (CRS) was observed in one patient in cohort 1 and one patient in cohort 2; the highest CRS grade was 2. Neurotoxicity was not observed. The infused huCART-meso cells were tolerated and generally safe with no related adverse events above grade 3. All subjects died before transitioning to long-term follow-up. For cohort 1, the three infused subjects were withdrawn from the study prior to transitioning to hospice. In cohorts 2 and 3, all six subjects died while on study, five of disease progression and one of acute kidney injury.

Clinical activity of huCART-meso in metastatic PDAC was limited. All nine subjects received the target dose of huCART-meso cells and were thus considered evaluable for response. In cohort 1 (i.v.), the best response was stable disease by Response Evaluation Criteria in Solid Tumors version 1.1 (RECIST1.1)[33] in 1 of 3 patients at the day 28 scans, but progressive disease was noted on scans at month 3 (Table 2). In cohort 2 (i.p.) and cohort 3 (i.h.), all patients had progressive disease by the day 28 scans. Median overall survival from infusion to date of death or date of last contact was 6.7 weeks (Figure 1B), and median progression-free survival was 3.9 weeks (Figure 1C).

The post-infusion kinetics of peripheral huCART-meso cell expansion and persistence are displayed in Figure 1D

CellPress
OPEN ACCESS

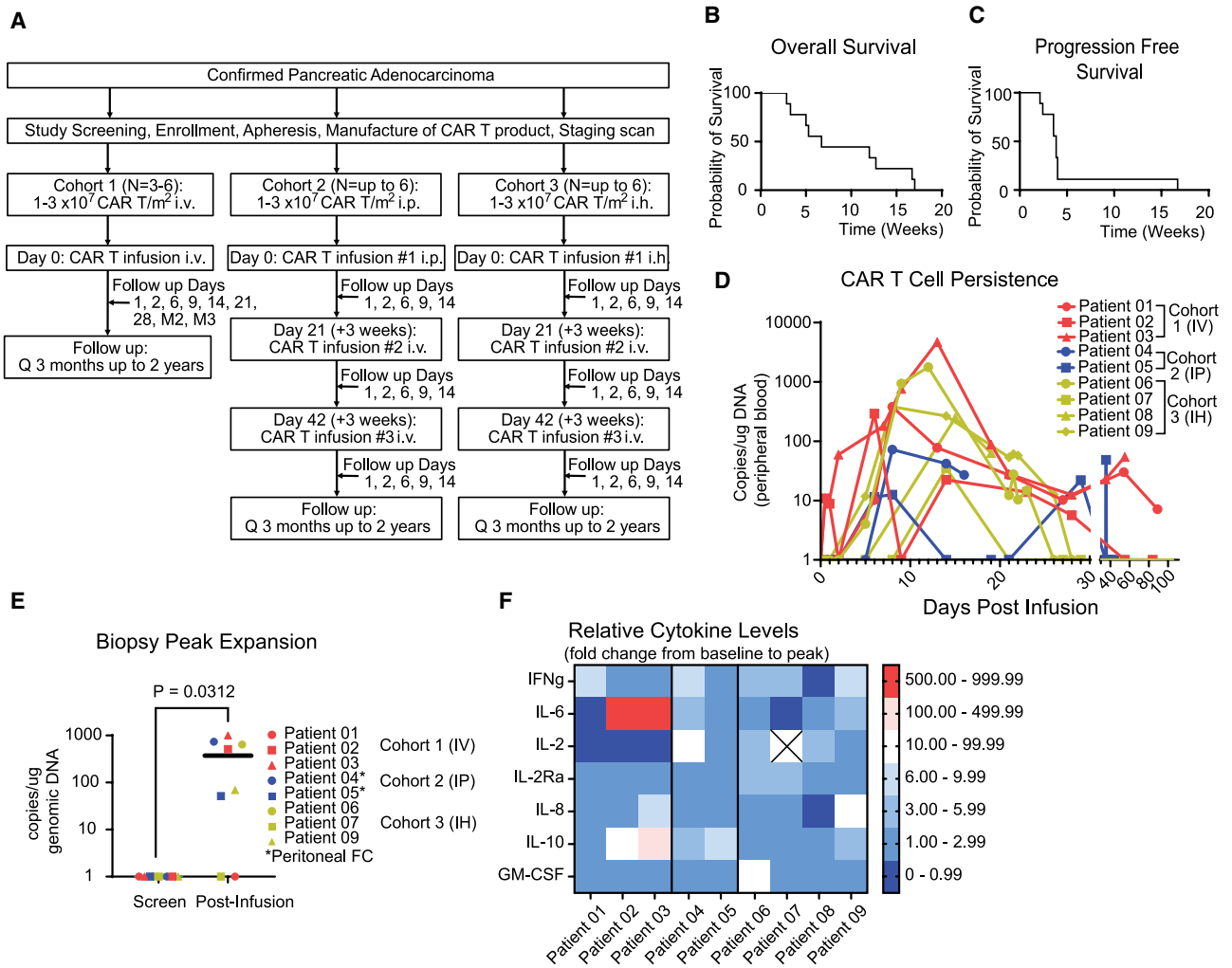


Figure 1. huCART-meso cells are tolerated and safe in a patient population with minimal cell expansion and cytokine response

(A) Protocol schema for screening, apheresis, T cell manufacture, treatment with huCART-meso cells, and follow-up. i.v., intravenous; i.p., intraperitoneal, i.h.; intrahepatic.

(B and C) (B) Overall survival and (C) progression-free survival of patients enrolled on the trial.

(D) huCART-meso cell engraftment in peripheral blood by qPCR-based detection of CAR-specific sequences in genomic DNA.

(E) huCART-meso cell expansion in pre- and post-infusion biopsy tissue samples by qPCR. Wilcoxon matched-pairs signed rank test, $n = 8$ patients.

(F) Heatmap grouped by cohort depicting fold changes in proinflammatory cytokine production from baseline/pre-CAR T cell infusion to the peak cytokine level post infusion. IL-2 levels for patient 07 were below the range of detection of the assay and are indicated as "X" in the figure.

See also Figure S1; Table S1.

(separated patient data in Figure S1A). huCART-meso cells were detected in all patients by quantitative PCR (qPCR) amplification of CAR-specific sequences in the genomic DNA. While peak levels of huCART-meso cells in circulation were similar, the persistence of huCART-meso cells in the blood was greater when CAR T cells were administered i.v. compared to local delivery. huCART-meso cells were also detected in biopsy and peritoneal fluid cells between days 13 and 26 in patients from all three cohorts (maximum expansion in Figure 1E and expansion per day in Figure S1B). Three patients (05, 06, and 09) on the local delivery cohorts received a subsequent i.v. infusion(s) of huCART-meso cells, but no additional expansion of CAR$^+$ cells occurred in circulation after this second infusion, and persistence dropped below the level of detection within 5 days in two of the three patients.

The kinetics of serum cytokines for 31 different analytes were assessed (Figure S1C) with further evaluation of six cytokines (IFNγ, interleukin [IL]-6, IL-2, IL-8, IL-10, and granulocyte-macrophage colony-stimulating factor [GM-CSF]) and the soluble IL-2 receptor, comparing the fold changes in cytokine production from baseline (pre-CAR T cell infusion) to the peak cytokine expansion (Figure 1F). Two patients in cohort 1 experienced a greater than 500-fold change in levels of IL-6 between pre- and post infusion; of these, one experienced

Table 1. All adverse events

Toxicity category	Grade 1	Grade 2	Grade 3	Grade 4	Grade 5	Total
Blood and lymphatic system disorders	**0**	**3**	**5**	**0**	**0**	**8**
Anemia	0	3	4	0	0	7
Disseminated intravascular coagulation	0	0	1	0	0	1
Cardiac disorders	**1**	**1**	**0**	**0**	**0**	**2**
Atrial fibrillation	0	1	0	0	0	1
Sinus tachycardia	1	0	0	0	0	1
Eye disorders	**0**	**1**	**0**	**0**	**0**	**1**
Blurred vision	0	1	0	0	0	1
Gastrointestinal disorders	**4**	**8**	**5**	**0**	**1**	**18**
Abdominal pain	1	2	0	0	0	3
Ascites	0	1	1	0	0	2
Constipation	0	2	0	0	0	2
Diarrhea	1	1	0	0	0	2
Duodenal obstruction	0	0	0	0	1	1
Gastrointestinal disorders – other (tongue white)	0	1	0	0	0	1
Gastroparesis	0	1	0	0	0	1
Ileal obstruction	0	0	1	0	0	1
Nausea	1	0	0	0	0	1
Obstruction gastric	0	0	2	0	0	2
Upper gastrointestinal hemorrhage	0	0	1	0	0	1
Vomiting	1	0	0	0	0	1
General disorders and administration site conditions	**5**	**3**	**3**	**0**	**4**	**15**
Fatigue	1	3	2	0	0	6
Fever	2	0	0	0	0	2
General disorders and administration site conditions – other (disease progression)	0	0	0	0	4	4
General disorders and administration site conditions – other (generalized edema)	0	0	1	0	0	1
General disorders and administration site conditions – other (night sweats)	1	0	0	0	0	1
Pain	1	0	0	0	0	1
Hepatobiliary disorders	**0**	**1**	**1**	**0**	**0**	**2**
Hepatic failure	0	0	1	0	0	1
Portal vein thrombosis	0	1	0	0	0	1
Immune system disorders	**1**	**1**	**0**	**0**	**0**	**2**
Cytokine release syndrome	1	1	0	0	0	2
Infections and infestations	**0**	**1**	**2**	**1**	**1**	**5**
Infections and infestations – other (thrush)	0	1	0	0	0	1
Lung infection	0	0	1	0	0	1
Peritoneal infection	0	0	0	0	1	1
Sepsis	0	0	1	1	0	2
Injury, poisoning, and procedural complications	**2**	**3**	**0**	**0**	**0**	**5**
Injury, poisoning, and procedural complications – other (citrate reaction)	2	3	0	0	0	5
Investigations	**8**	**5**	**8**	**3**	**0**	**24**
Alanine aminotransferase increased	2	0	0	0	0	2

(*Continued on next page*)

CellPress
OPEN ACCESS

Table 1. ***Continued***

Toxicity category	Grade 1	Grade 2	Grade 3	Grade 4	Grade 5	Total
Alkaline phosphatase increased	0	0	1	0	0	1
Aspartate aminotransferase increased	0	1	0	0	0	1
Blood bilirubin increased	0	1	1	0	0	2
Creatinine increased	2	0	0	0	0	2
Fibrinogen decreased	1	0	0	0	0	1
INR increased	1	1	0	0	0	2
Lymphocyte count decreased	1	1	4	2	0	8
Neutrophil count decreased	0	0	1	0	0	1
Platelet count decreased	0	0	1	1	0	2
White blood cell decreased	1	1	0	0	0	2
Metabolism and nutrition disorders	**9**	**12**	**5**	**0**	**0**	**26**
Anorexia	1	3	0	0	0	4
Dehydration	0	3	0	0	0	3
Hyperglycemia	0	0	1	0	0	1
Hyperuricemia	1	0	0	0	0	1
Hypoalbuminemia	2	5	0	0	0	7
Hypocalcemia	2	0	0	0	0	2
Hypokalemia	0	1	1	0	0	2
Hyponatremia	3	0	2	0	0	5
Tumor lysis syndrome	0	0	1	0	0	1
Musculoskeletal and connective tissue disorders	**1**	**4**	**0**	**0**	**0**	**5**
Back pain	0	3	0	0	0	3
Bone pain	0	1	0	0	0	1
Flank pain	1	0	0	0	0	1
Nervous system disorders	**3**	**1**	**3**	**0**	**0**	**7**
Encephalopathy	0	0	1	0	0	1
Headache	2	0	0	0	0	2
Nervous system disorders – other (confusion, expressive aphasia secondary to brain metastases)	0	0	1	0	0	1
Nervous system disorders – other (foot drop)	1	0	0	0	0	1
Paresthesia	0	1	0	0	0	1
Stroke	0	0	1	0	0	1
Psychiatric disorders	**2**	**3**	**0**	**0**	**0**	**5**
Anxiety	0	1	0	0	0	1
Confusion	1	1	0	0	0	2
Delirium	1	1	0	0	0	2
Renal and urinary disorders	**0**	**0**	**0**	**0**	**1**	**1**
Acute kidney injury	0	0	0	0	1	1
Respiratory, thoracic, and mediastinal disorders	**2**	**2**	**5**	**0**	**0**	**9**
Cough	1	0	0	0	0	1
Dyspnea	1	0	1	0	0	2
Hypoxia	0	2	4	0	0	6
Skin and subcutaneous tissue disorders	**1**	**0**	**0**	**0**	**0**	**1**
Skin and subcutaneous tissue disorders – other (raised areas underneath skin)	1	0	0	0	0	1

(*Continued on next page*)

Table 1. *Continued*

Toxicity category	Grade 1	Grade 2	Grade 3	Grade 4	Grade 5	Total
Vascular disorders	**4**	**2**	**1**	**1**	**0**	**8**
Flushing	1	0	0	0	0	1
Hematoma	2	0	0	0	0	2
Hypotension	0	1	1	1	0	3
Thromboembolic event	1	1	0	0	0	2
Total	**43**	**51**	**38**	**5**	**7**	**144**

grade 2 clinical CRS. In cohorts 2 and 3, minimal changes in the levels of various analytes were observed between pre- and post-infusion time points, consistent with the low peak expansion of cells.

Cellular analyses reveal a cold-tumor phenotype and limited T cell infiltration in the metastases of locally infused patients

Tumor tissue from metastatic lesions and peritoneal fluid were collected in patients for further analysis (Table 3). Fine needle aspirates of metastatic lesions were collected pre- and post therapy to interrogate the underlying mechanisms of resistance to CAR T cell therapy in PDAC. Flow cytometry was performed on cells isolated from treatment biopsies of patient 05 (cohort 2) and liver metastasis from patients in cohort 3, except for patient 08, from whom day 14 post-infusion sample was not collected for clinical reasons. We monitored changes in T cells ($CD3^+$/$CD4^+$ and $CD8^+$), natural killer (NK) ($CD56^+CD3^-$), NK T ($CD56^+CD3^+$), B cells ($CD19^+CD3^-CD45^+$), monocytes ($CD14^+CD3^-CD45^+$), and erythroid progenitor ($CD45^+CD235a^+$) subsets and surface CAR expression on T cells and MSLN expression on $EpCAM^+$ cells (Figure S2A). We observed low $CD3^+$ T cell infiltration at baseline and at day 14 post infusion indicating a persistent cold-tumor phenotype (Figures S2B and S2C). However, despite low infiltration, in patients from whom day 14 post-infusion samples could be collected, there was an increase in the $CD3^+$ population compared to baseline (Figure S2C) ($p = 0.0124$, $p = 0.0392$, and $p = 0.0159$ for patients 05, 06, and 09, respectively). Despite this increase in T cells, flow cytometry analysis using a CAR-specific anti-idiotypic antibody to detect surface CAR expression revealed no CAR staining in the metastatic tissue (Figure S2D and data not shown for patient 07 due to complete absence of immune cells in the biopsy sample analyzed). This observation correlated with the low CAR vector copy number detected in the blood and liver tissue from cohort 3 patients at the same time points (Figure S2E). Interestingly, in contrast to flow analyses in patient 06 (Figure S2D), qPCR detection of CAR revealed high levels of CAR T cells in the peripheral blood and in the day 14 liver biopsy (Figure S2E), potentially indicating CAR downregulation in the tissue and blood.[26,34]

MSLN protein levels were assessed in patients 05, 07, and 09 by flow cytometry (Figures S2F and S2G). We detected decreased $MSLN^+EpCAM^+$ viable tumor cells in post-infusion samples in two out of three patients (Figures S2F and S2G). However, patients 05 and 06 displayed a minor frequency (<1%) of $MSLN^+EpCAM^+$ cells in the metastatic tissue collected at baseline (Figures S2F and S2G). Taken together, poor infiltration of both endogenous non-transduced and huCART-meso cells into the metastases was observed along with limited persistence; however, a decrease in MSLN protein levels was observed in patients 05 and 09.

huCART-meso cells acquire an exhausted T cell phenotype after infusion into the ascites fluid

To better characterize the intratumoral huCART-meso cells, we collected ascites fluid from patients 04 and 05 (cohort 2) following i.p. infusion (Figure 2A). Notably, despite the local delivery of huCART-meso cells into the peritoneal fluid, we observed either low levels of T cells expressing the CAR on the surface at day 7 (Figure 2B) or no surface CAR expression on T cells (Figure S2H) although the transduction efficiency of the

Table 2. Response data of patients

Subject ID	Cohort	Days post infusion	Total target tumor response	Total non-target tumor response	Overall tumor response
Patient 01	1	day 28	stable disease	progressive disease	progressive disease
Patient 02	1	day 28	stable disease	progressive disease	progressive disease
Patient 03	1	day 28	stable disease	stable disease	stable disease
Patient 03	1	month 3	progressive disease	progressive disease	progressive disease
Patient 04	2	day 23	progressive disease	not evaluable	progressive disease
Patient 05	2	day 25	progressive disease	progressive disease	progressive disease
Patient 06	3	day 28	progressive disease	progressive disease	progressive disease
Patient 06	3	month 3	progressive disease	progressive disease	progressive disease
Patient 07	3	day 27	progressive disease	progressive disease	progressive disease
Patient 08	3	day 19	progressive disease	stable disease	progressive disease
Patient 09	3	day 25	progressive disease	progressive disease	progressive disease

Table 3. Samples collected from patients

Cohort	Subject ID	Sample type	Trial time point	Analysis performed
C2 (intraperitoneal)	patient 04	peritoneal fluid	day 0, day 7	flow cytometry
C2 (intraperitoneal)	patient 04	peritoneal fluid	day 7	scRNA-seq
C2 (intraperitoneal)	patient 05	peritoneal Met (FNA)	day 0, day 14	flow cytometry
C2 (intraperitoneal)	patient 05	peritoneal fluid	day 26	scRNA-seq
C3 (intrahepatic)	patient 06	liver met (FNA)	day 0, day 14	flow cytometry
C3 (intrahepatic)	patient 07	liver met (FNA)	day 0, day 14	flow cytometry
C3 (intrahepatic)	patient 08	liver met (FNA)	day 0	flow cytometry
C3 (intrahepatic)	patient 09	liver met (FNA)	day 0, day 14	flow cytometry

FNA, fine needle aspirate; C2, cohort 2; C3, cohort 3; Met, metastasis.

corresponding products was 39.5% and 22.0%, respectively. This observation aligned with low levels of CAR copies detected in the blood and peritoneal fluid of both patients (Figures 2C and 2D), indicating low persistence of the infused CAR T cells in the peritoneal fluid of these patients. Next, we performed single-cell RNA sequencing (scRNA-seq) on $CD3^+$ T cells sorted from the peritoneal biopsies on days 7 and 26 post CAR T infusion and integrated the samples for analysis (Figures S2I and S2J). Canonical marker genes were used to identify T cell subsets (Figure 2E). CD4 T cell subsets clustered on the left, and CD8 T cell subsets clustered on the right (Figure 2E). In the CD4 population, we detected regulatory T cells (Tregs; FOXP3, IL2RA, and IKZF2),[35] naive T cells (SELL, CCR7, and LEF1),[35,36] and effector memory T cells (Tem; IL7R and KLRB1)[37] (Figure 2E). In the CD8 population, we detected memory T cells (CCR7, LEF1, SELL, IL7R, and TCF7),[38] Tem (IL7R, KLRG1, and NKG7),[39,40] $GZMK^+$ effector memory T cells ($GZMK^+$ Tem; GZMK, NKG7, PRF1, GZMH, and CCL5),[41] terminally differentiated Tem (NKG7, PRF1, GZMH, and CCL5),[42] and NK-like T cells (NK-like; NCAM1, FCGR3A, GNLY, GZMB, KLRC1, and KLRC2)[41] (Figure 2E). We additionally detected a $CD3^+$ cluster (defined as unknown) that uniquely expresses several calcium-binding proteins (S100A8 and S100A9) and complement proteins (C1QB and C1QA). While the peritoneal fluid consists of mostly endogenous T cells, we detected T cells expressing huCART-meso RNA in the TME via scRNA-seq using ALRA imputation (Figure 2F). We detected 380 huCART-meso-positive cells (CARpos) in patient 04 and 157 cells in patient 05. Next, we downsampled the endogenous CAR-negative (CARneg) dataset to have an equal number of CARpos and CARneg T cells. We examined the differences in T cell subset distribution between CARpos and CARneg T cells and found that CARpos cells were enriched in the CD8 $GZMK^+$ Tem cluster and depleted in the CD4 naive cluster (Figure 2G). Together, our data characterizing T cells in malignant ascites suggest that CAR T cells post infusion display a unique T cell distribution profile that differs from endogenous CARneg T cells; however, increased replicates would strengthen this dataset.

In our previous study,[26] we identified a 30-gene dysfunction signature in huCART-meso cells chronically exposed to tumor antigen *in vitro*. Strikingly, 19/30 of the dysfunction signature genes were highly expressed in CARpos cells compared to CARneg cells in the patient samples, including the transcription factors SOX4 and ID3 (Figure 2H). Of note, NK receptor genes (KLRB1, KLRC1, KLRC2, and KLRD1) were not upregulated in the patient CAR T cells (Figure 2H), agreeing with earlier data (see Figure 2G). Other T cell exhaustion genes not described in our 30-gene signature were increased in the patient CARpos T cells (CTLA4, TIGIT, and PDCD1) (Figure 2I, select dysfunction signature genes also shown for comparison). Taken together, huCART-meso cells obtained from patient biopsies post CAR T cell infusion express common T cell exhaustion markers and the huCART-meso dysfunction signature as previously described,[26] including the transcription factors ID3 and SOX4. This finding indicates that the *in vitro* model replicates many but not all features of CAR T cell dysfunction *in vivo*.[26]

Donor characteristics influence the *in vivo* efficacy of single ID3 or SOX4KO huCART-meso cells

Our previous findings systematically investigated the drivers of CAR T cell exhaustion; we found that the transcriptional regulators ID3 and SOX4 were upregulated following chronic antigen exposure and that genetic deletion of each transcription factor demonstrated improved cytotoxicity compared to wild-type (WT) CAR T cells in chronic activation settings *in vitro*.[26] Since huCART-meso cells isolated from the peritoneal fluid of locally infused patients upregulated ID3 and SOX4, and due to their significant upregulation in exhausted CAR T cells and prior validation *in vitro*,[26] we hypothesized that the acquisition of a dysfunctional phenotype in CAR T cells occupying the TME might contribute to the observed lack of efficacy in the clinic.

To evaluate whether ID3KO and SOX4KO huCART-meso cells have improved *in vivo* killing, we manufactured huCART-meso ID3 or SOX4KO cells from healthy donor T cells with a high editing efficiency (Figures S3A and S3B). KO CAR T cells showed no differences in viability, population doublings, or cell volume compared to WT huCART-meso cells (Figure S3C). To evaluate the antitumor efficacy of these KO CAR T cells in a xenograft mouse model, suboptimal doses of WT or KO huCART-meso cells were i.v. injected once tumors reached ~250 mm^3 (Figure 3A), allowing a stringent challenge of the CAR T cells *in vivo*. Although improved responses were observed in KO CAR T cell groups in some donors (Figure 3B, suboptimal doses for ND561 were 1×10^6 CAR T/mouse), without significant differences in body weights (Figure 3C), the observed therapeutic benefit was highly variable among CAR T cell products.

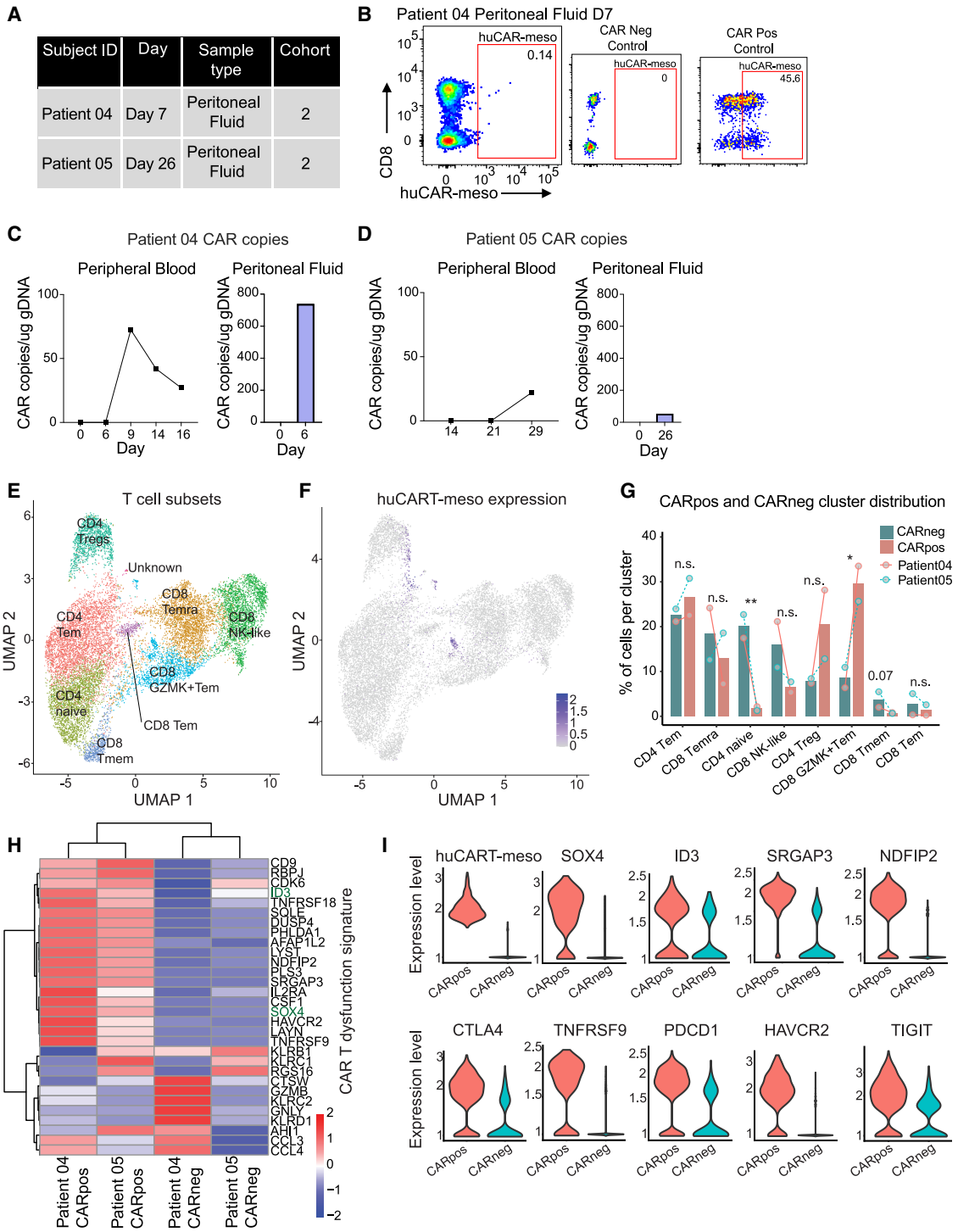


Figure 2. Locally delivered huCART-meso cells are enriched for GzmK$^+$ Tem phenotypes and exhibit a dysfunctional T cell phenotype including upregulation of SOX4 and ID3

(A) Summary of the samples collected for flow cytometry and scRNA-seq analyses.

(B) Representative flow cytometry plot of patient 04 showing detection of peritoneal fluid infiltrating CD3$^+$ cells with surface expression of the huCART-meso.

(C and D) CAR detection performed by qPCR on peripheral blood (left) and peritoneal fluid (right) of patient 04 (C) and patient 05 (D).

(E) UMAP projection of scRNA-seq data from sorted CD3$^+$CD45$^+$ cells infiltrating the peritoneal fluid 7 days post intraperitoneal infusion (patient 04) or 26 days post infusion (patient 05). UMAP plot is labeled with T cell subsets.

(legend continued on next page)

Intriguingly, SOX4KO CAR T cells consistently demonstrated better antitumor efficacy compared to ID3KO CAR T cells (Figure 3B). Thus, we further explored this variability in antitumor efficacy in SOX4KO huCART-meso cells compared to WT (Figure 3D). CAR T cell products were classified into good, intermediate, and non-responders based on the improvement observed with SOX4KO CAR T cells (Figure 3E). Experiments with donors of different categories were performed together to rule out cofounding effects in the mouse colony. Curative doses were repeated in independent experiments to rule out batch effects on CAR T cells. Various factors were evaluated to identify associations with *in vivo* primary response across donors, including cell source (frozen vs. fresh), total cells injected, population doublings at manufacturing, surface CAR expression, age, and reported gender, among others. However, none reached statistical significance (Table S2). Additionally, to investigate if the memory phenotype of the manufactured product was associated with *in vivo* primary responses, we measured CCR7/CD45RO phenotypes using flow cytometry (Figure 3F) and found no association. Similar distributions were observed across the different subpopulations between the WT and KO groups; however, there was variability across donors within the effector memory (EM) and central memory (CM) subpopulations denoted by the wide sample distribution (Figure 3F).

Taken together, single SOX4 and, to a lesser extent, single ID3KO CAR T cells improve efficacy *in vivo.* However, the observed variability underscores the complex interplay of CAR T cell product characteristics, including donor variability influencing therapeutic outcomes upon ID3 or SOX4KO.

Mice injected with single KO of SOX4 or ID3 eventually experience tumor recurrence

Some WT and KO huCART-meso-treated mice that initially cleared tumors relapsed at the primary tumor site, beginning approximately 2 months after CAR T infusion (Figures S3D and S3E). To dissect factors contributing to the therapeutic failure of CAR T cells, we worked by exclusion to analyze relapsing tumors from mice treated with WT or SOX4KO huCART-meso cells (Figure 4A). T cells infiltrating the recurrent tumors displayed ~98% editing efficiency at the SOX4 locus, excluding the possibility of low persistence of the KO cells (Figure 4B). Next, we analyzed recurrent tumor-infiltrating human T cells (TILs) in recurrent tumors using flow cytometry, from donor ND561, which was a good responder (see Figure 3E, left). Notably, abundant TILs were detected within the tumors, ruling out issues related to non-persistence (Figure 4C). Recurrent tumors from mice initially injected with SOX4KO huCART-meso cells may show a slightly higher level of T cell infiltration compared to WT controls (Figure 4C, left; Figure S4A). Interestingly, both WT and SOX4KO CAR T cells demonstrated reduced levels of surface CAR expression compared to the infused product (Figure 4C, right), suggesting surface CAR downregulation; however, SOX4KO CAR T cells from recurrent tumors had a higher number of surface CAR^+ T cells than WT (Figure 4C, right). Furthermore, surface expression of MSLN on recurrent tumor cells was confirmed, ruling out the possibility of escape due to antigen loss, although more $MSLN^-EPCAM^+$ cells were found in the SOX4KO CAR T-treated recurrent tumors (Figure 4D).

To investigate mechanisms underlying tumor recurrence, we sorted the $CD8^+$ T cells infiltrating the relapsing tumors and performed scRNA-seq. Samples were plotted onto uniform manifold approximation and projection (UMAP) space, and integrated samples did not show major differences in cluster distribution (Figures 4E and S4B). Next, we identified T cell subsets using the expression of canonical T cell marker genes (Figure 4F). Seurat identified 11 cell clusters that broadly fit into two main T cell subsets: an NK-like T cell exhaustion subset dominated by cluster 2 (Figure 4F, NK-like Tex; on left) and a $GZMK^+$ T cell exhaustion subset that consists of all the remaining clusters (Figure 4F, $GZMK^+$ Tex; on right). All clusters expressed high levels of canonical T cell exhaustion markers (LAG3, HAVCR2, TOX, and TIGIT) (Figure S4C) and lacked expression of memory markers (IL7R and CCR7) (Figure S4D). The $GZMK^+$ Tex subset expressed high levels of GZMK and EOMES, a T-box transcription factor that has been linked to T cell exhaustion[43] (Figure S4E). The NK-like Tex subset expressed high levels of NK receptor genes (KLRC1, KLRC2, KLRB1, and KLRD1) (Figure S4F) and, of interest, uniquely expressed high levels of genes found in our 30-gene CAR T dysfunction signature identified from *in vitro*-stimulated CAR T cells, including TNFRSF18, RGS16, CD9, and SRGAP3 (Figure S4G). Of note, 56% of TILs extracted from the recurrent tumors expressed the CAR (Figure 4G), and thus low persistence did not explain the delayed failure of tumor control. Taken together, two distinct CAR T cell exhaustion clusters arise in mice that experience tumor recurrence: one characterized by the expression of dysfunction-associated NK receptors, and one characterized by GZMK and EOMES.

In the recurrent tumor model, SOX4KO CAR T cells did not protect against tumor recurrence compared to WT CAR T cells (Figure S3D). Nonetheless, we were interested if genomic differences between the KO and WT groups could be identified at the molecular level. We found that WT and

(F) huCART-meso expression associated with (E).
(G) Distribution of huCAR-meso+ (CARpos) and endogenous CAR-negative T cells (CARneg) across cell type clusters defined in (E). Unknown cluster from (E) was excluded. The *y* axis represents the percent of cells found within each cell type cluster, calculated by taking the number of cells per condition (condition being CARpos or CARneg) within each cell type cluster and dividing by the total number of cells in that condition, calculated for each patient individually. Dots represent the individual patient values, and the bar plot represents the average of the patient values; moderated t test via the propeller method ($n = 2$ patients). *p* values denoted as $^*p < 0.05$ and $^{**}p < 0.01$.
(H) Expression of the 30-gene CAR T dysfunction signature[26] in $CD3^+$ CARpos and CARneg T cells of patients 04 and 05 post infusion.
(I) Gene expression levels of huCART-meso, SOX4, ID3, SRGAP3, NDFIP2, CTLA4, TNFRSF9, PDCD1, HAVCR2, and TIGIT in CARpos (left, red) and CARneg cells (right, green). CARneg cells were randomly downsampled to have an equal number of CARpos and CARneg cells for analyses in (G)–(I).
See also Figure S2.

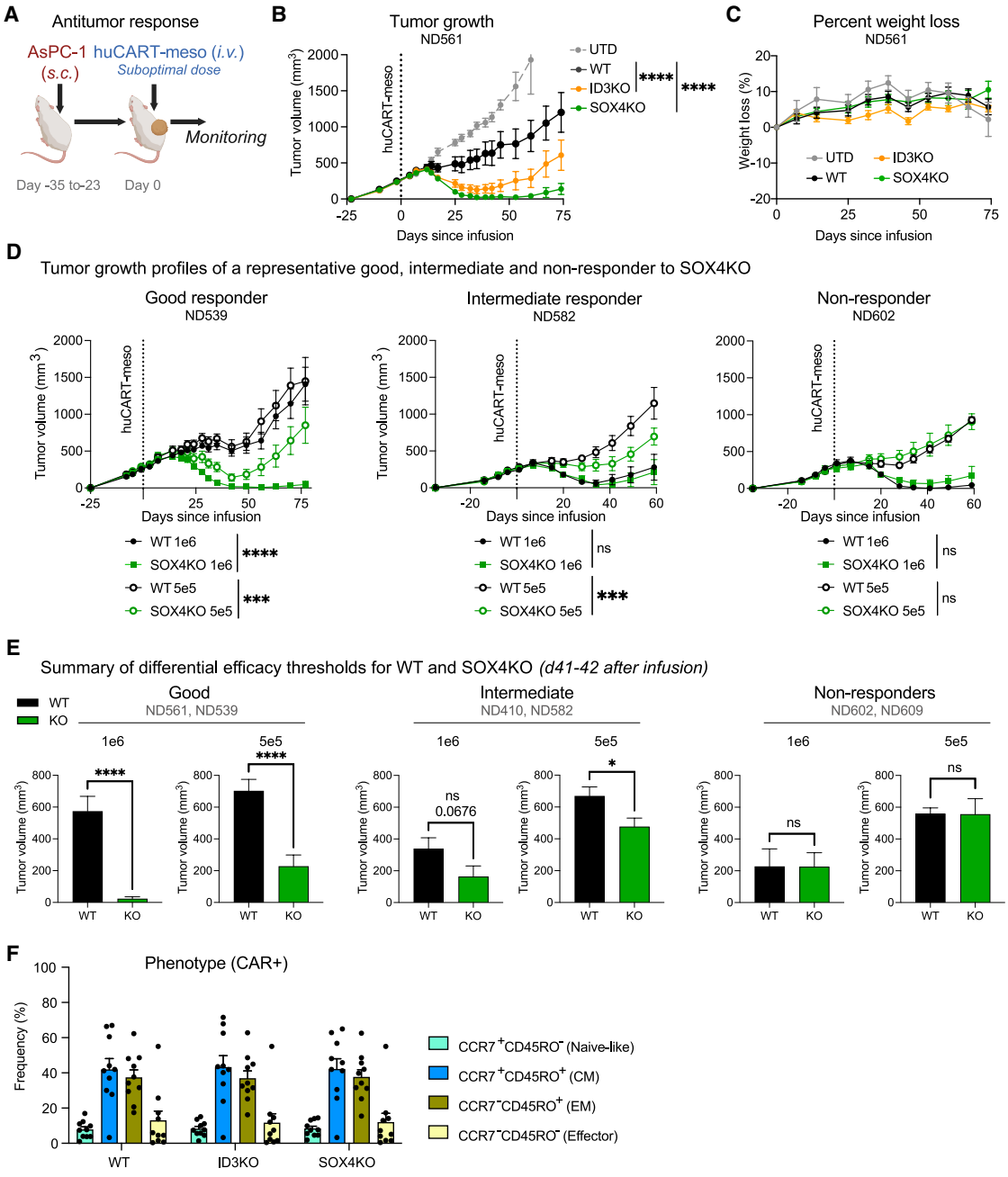


Figure 3. Single KO of ID3KO or SOX4KO in huCART-meso cells induces variable antitumor primary responses

(A) Experimental design to evaluate the efficacy of ID3KO and SOX4KO huCART-meso cells in AsPC-1 tumor-bearing mice. Suboptimal doses of huCART-meso cells were injected i.v. when tumors reached ~250–300 mm^3 (day 0, n = 7–12 mice per group).

(B) Tumor growth volumes of AsPC-1 tumor-bearing mice treated with 1×10^6 WT, ID3KO, or SOX4KO ND561 huCART-meso cells or with UTD (untransduced T cells) at equivalent amounts of total cells; two-Way ANOVA with Geisser-Greenhouse correction and Dunnett's post hoc test; mean ± SEM (n = 8–11 mice per group). Dashed line indicates the day of infusion. This result is representative of three independent experiments performed with CAR T cells derived from three different donors.

(C) Percentage of weight loss of mice infused with UTD, WT, ID3KO, or SOX4KO ND561 huCART-meso cells; mean ± SEM.

(D) Tumor growth profiles of a representative good (ND539), intermediate (ND582), and non-responder (ND602) compared to mice treated with WT (black) or SOX4KO huCART-meso cells (green). 1×10^6 and 5×10^5 CAR T cells/mouse administered; two-way ANOVA with Geisser-Greenhouse correction; mean ± SEM (n = 5–11 mice per group).

(E) Tumor volumes of representative WT and SOX4KO huCART-*meso*-treated mice at day 41–42 after infusion. Two donors were used per group. Good responders: n = 7–11 animals per donor, totaling 16–21 animals per group and CAR T dose; intermediate responders: n = 5–9 animals per donor, totaling 13–14

(legend continued on next page)

SOX4KO recurrent tumor TILs did not differ in their cluster distribution (Figure 4H), suggesting that SOX4KO did not impact T cell trajectories in the setting of tumor recurrence. However, additional replicates would strengthen this dataset. Further, common exhaustion markers (TNFRSF9, TIGIT, LAG3, and HAVCR2) were highly expressed in WT and SOX4KO T cells harvested from recurrent tumors (Figure 4I). Our data suggest that SOX4KO CAR T cells can delay but not prevent CAR T cell exhaustion *in vivo*.

Double KO of SOX4 and ID3 in huCART-meso cells provides sustained protection against tumor recurrence

Considering that both ID3 and SOX4 were upregulated in exhausted cells and the single-KO CAR T cells experienced tumor relapse, we sought to investigate whether simultaneous KO of SOX4 and ID3 genes would improve antitumor responses and long-term protection from relapse. We generated WT, single-KO, and double-KO (DKO) CAR T cells from seven healthy donors and achieved high levels of editing efficiency (Figure S5A). DKO CAR T cells exhibited no difference in proliferation as assessed by population doublings, cell volume, or viability during expansion compared to WT and single KOs (Figure 5A), and no differences were observed in the T cell subset distribution between the groups following expansion (Figure S5B). Further analysis of the DKO revealed that while the majority of the cells were central memory and effector memory phenotypes, donor-dependent differences were observed in the distribution of T cell phenotypes (Figure 5B).

To assess the antitumor efficacy of DKO CAR T cells, suboptimal doses of WT, single-KO, or DKO CAR T cells were injected into AsPC-1 tumor-bearing mice. DKO CAR T cells demonstrated comparable antitumor efficacy to single KOs at suboptimal doses (ND584, 5×10^5 CAR T cells per mouse, Figure 5C), again with no impact on weight (Figure 5D), indicating that the double KO of SOX4 and ID3 did not improve the antitumor efficacy of CAR T cells. Next, we evaluated the efficacy of DKO CAR T cells in preventing relapse after an initial response. AsPC-1 tumor-bearing xenografts were injected with optimal doses of WT, single-KO, and DKO CAR T cells, and mice were monitored for relapse (Figure 5E). We observed that several mice in the WT and single-KO arms relapsed at early time points, starting around 2 months after tumor inoculation. In contrast, DKO-treated mice experienced fewer and delayed relapses or remained relapse-free by the end of the study (1×10^6 CAR T cells per mouse; ND528, Figure 5F; ND584, Figure S5C), and for those that did relapse, tumor volumes in DKO CAR T-treated mice were significantly reduced at the end of the study (Figure 5G). Next, we combined all *in vivo* studies into one statistical analysis, which demonstrate that mice treated with DKO CAR T cells showed long-term antitumor efficacy with significant increased relapse-free survival (RFS) compared to WT counterparts (Figures 5H and 5I; Table 4).

DISCUSSION

This phase 1 study investigated the safety and feasibility of huCART-meso therapy in patients with advanced PDAC and found limited clinical response. Given this, we conducted an in-depth analysis of tumor-infiltrating CAR T cells from patients with PDAC to understand resistance mechanisms in the pancreatic cancer microenvironment, providing valuable insights into their behavior in solid tumors.

Following our prior work with murine-derived anti-MSLN SS1 CAR T cells,[16,17] we developed a fully human anti-MSLN CAR construct with a CD3ζ/4-1BB costimulatory domain targeting a membrane-proximal epitope, which has been reported to enhance activity.[44] Autologous huCART-meso cells were administered via three different delivery strategies: systemic i.v. infusion (cohort 1), or regionally either into the peritoneal fluid (cohort 2) or via i.h. artery infusion (cohort 3) for patients with peritoneal and liver metastases, respectively. Our findings demonstrated that i.v. and regional delivery strategies were feasible, with no related adverse events above grade 3. The overall safety of i.p. and i.h. administration aligns with previously published reports on regional CAR T cell delivery.[45,46] Of note, i.v. delivery was complicated by pneumonitis in patients with moderate pulmonary metastatic burden, consistent with prior observations in mesothelioma and ovarian cancer trials using the same CAR T construct at higher doses.[32] Pneumonitis was not observed when huCART-meso cells were delivered regionally or i.v. in patients with low or no pulmonary metastases.

Despite encouraging safety results, the best response observed was transient stable disease in a single patient of cohort 1. This limited clinical efficacy could be explained by a number of factors. First, huCART-meso cells are present at low to moderate levels in blood and tumor metastases, with limited expansion with subsequent infusions. Second, although we confirmed CAR T cell trafficking into metastases following hepatic artery infusion (consistent with prior reports using i.h. delivery[47]), the levels of CAR T cells detected in the metastases were lower than those reported in other solid tumor trials, such as with CAR T-PSMA-TGFβRDN cells in metastatic prostate cancer or IL15-GPC3-CAR T cells in patients with GPC3-positive cancers.[48,49] Our findings align with other clinical trials targeting MSLN[16,17] and CD133,[50] where safety was achieved, but efficacy was modest. Together, this underscores the need to enhance T cell persistence and expansion within the TME.

We observed a decrease in $MSLN^+Epcam^+$ tumor cells in two out of three patients whose metastatic lesions were analyzed for MSLN expression, suggesting some degree of on-target CAR T cell activity. However, baseline MSLN expression was heterogeneous among patients, and its decrease post infusion may have been influenced by MSLN protein shedding[51] or sampling variability in different metastatic sites.

Consistent with previous reports, we observed low infiltration of endogenous T cells at baseline in the metastases of all

animals per group and CAR T dose; non-responders: $n = 3–5$ animals per donor, totaling 5–8 animals per group and CAR T dose; t test or Mann-Whitney test (for non-normally distributed data); mean ± SEM.

(F) Post-expansion phenotype huCART-meso cells derived from healthy donors.

$^{****}p < 0.0001$, $^{***}p < 0.001$,$^{*}p < 0.05$, ns: not significant. See also Figure S3; Table S2.

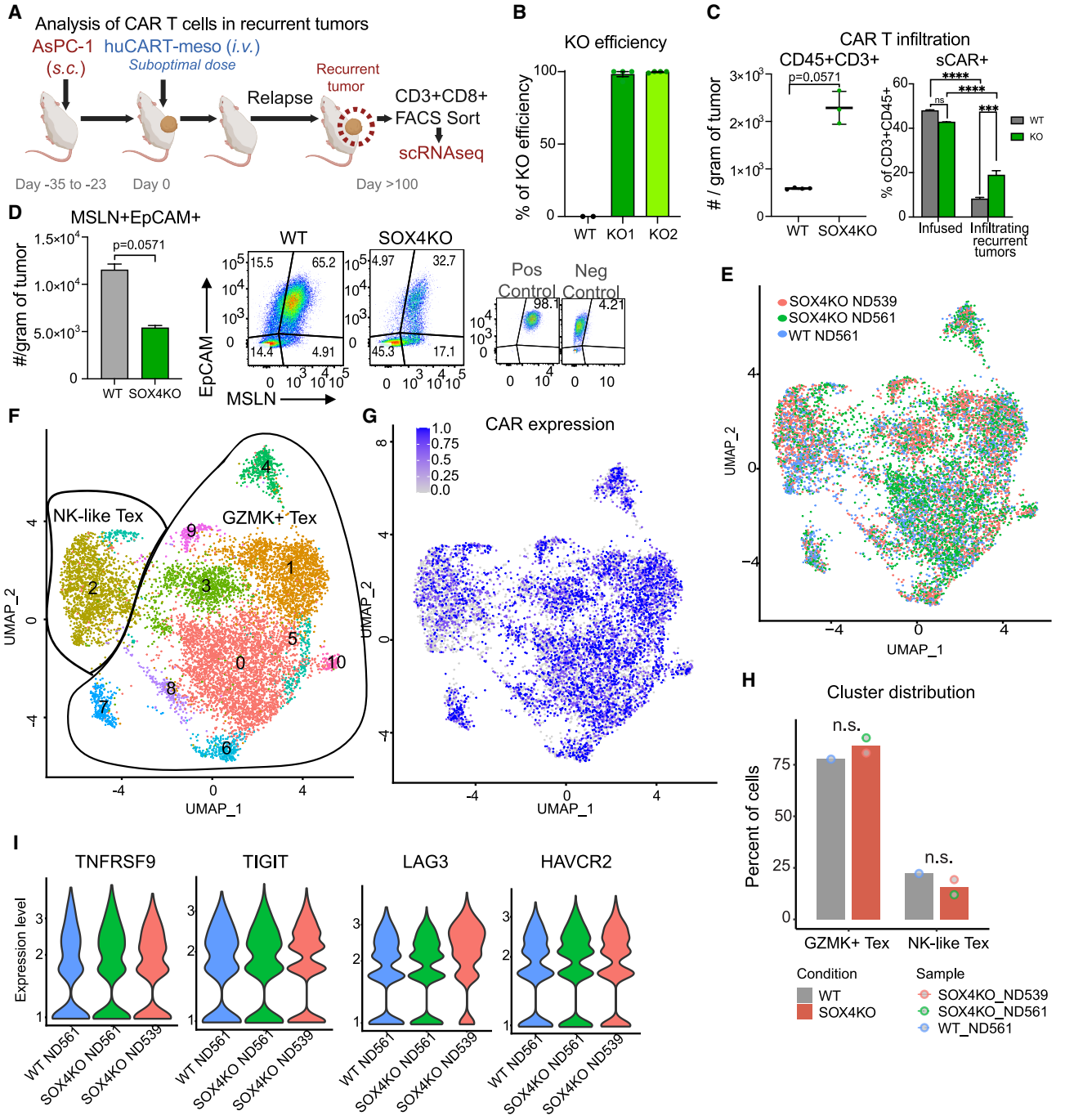


Figure 4. Mice injected with single KO of SOX4 or ID3 eventually experience tumor recurrence

(A) Experimental design for recurrent tumor model.

(B) KO efficiency in sorted T cells from relapsing tumors. Each dot represents a technical replicate (independent sequencing for KO assessment from one mouse per group); mean ± SEM.

(C) $CD3^+CD45^+$ T cell infiltration in ND561 WT and SOX4KO relapsing tumors (left) and percent of $CD3^+CD45^+$ surface huCART-meso in relapsing tumors and infused products (right). Each dot represents a technical replicate (n = 1 mouse per group); Mann-Whitney U test (left) and two-Way ANOVA and Sidak post hoc test (right); mean ± SEM.

(D) Total number of $MSLN^+Epcam^+$ cells (#) per gram of tumor (left) and representative flow cytometry plots (right) of MSLN expression in ND561 WT and SOX4KO-treated relapsing tumors (n = 1 mouse per group). AsPC-1 cells were used as positive control and MSLN minus as negative control for MSLN staining; Mann-Whitney U test. Error bars represent variation between technical replicates; mean ± SEM.

(legend continued on next page)

patients analyzed, indicative of a cold-tumor phenotype.[52] Notably, all patients showed increased endogenous CD3$^+$ T cell populations post infusion, suggesting that huCART-meso therapy may have stimulated endogenous T cell expansion, a phenomenon previously observed.[53] Additionally, flow cytometry revealed no surface expression of the chimeric receptor in the metastatic biopsies from patients in cohorts 2 and 3, possibly due to limited sample material, heterogeneous MSLN expression,[54] low infiltration, or downregulation of surface CAR expression due to trogocytosis or chronic antigen exposure.[55–59]

To further investigate the molecular basis of this limited efficacy, we performed scRNA-seq on post-infusion CAR T cells obtained from the peritoneal fluid. This analysis revealed a transcriptional phenotype consistent with chronic activation-induced dysfunction, including the upregulation of transcriptional regulators such as SOX4 and ID3,[26] which have been implicated in T cell exhaustion. Compared to endogenous T cells, huCART-meso cells displayed enrichment for a CD8 GZMK$^+$ phenotype following local delivery, which has been associated with limited cytotoxic potential[60] and immune aging[61,62] and was found to be an intermediate state between effector and exhausted T cells.[41] Furthermore, while not significant, we observed a higher frequency of the CD4$^+$ Treg phenotype, suggesting an immunosuppressive effect that may have further hindered CAR T cell function.[63] CAR T cells with a Treg phenotype have been reported in non-responders to CAR19 therapy for large B cell lymphomas,[63,64] where increased CAR Treg populations were linked to disease relapse.[64] It remains unclear if the observed T cell subsets are present in the infusion product or if they differentiated due to exposure in the TME. In either case, this shift in T cell phenotype may impact and limit the efficacy of huCART-meso cell activity, activation, and expansion in patients. While these samples provide valuable information, it is important to note that the number of patients analyzed was limited and that prior treatments varied in type and number across individuals. These factors should be considered when interpreting the findings.

To enhance huCART-meso efficacy, we targeted transcription factors linked to T cell exhaustion. Our previous work showed that knocking out SOX4 or ID3 improves effector function following chronic antigen stimulation *in vitro*,[26] consistent with other cancer models linking SOX4 and ID3 to T cell exhaustion.[41,65–67] In the present study, anti-MSLN CAR T cells with single KOs showed strong but donor-dependent benefits *in vivo*, suggesting that larger sample sizes are needed to clarify phenotype-response correlations. Variable responses may result from functional redundancy among SOX and ID family members,[68,69] genetic compensation,[70] or donor-specific non-heritable characteristics.[71,72] This variability emphasizes the need to account for patient-specific traits when optimizing CAR T therapies. Recent studies in CD19 CAR T cells have suggested that a Th2-skewed phenotype in the pre-infusion products correlates with improved long-term responses,[73] potentially adding another layer of complexity to donor-specific therapeutic outcomes. The intricate interplay between genetic modifications and baseline donor characteristics underscores the importance of understanding donor-specific factors for improved outcomes. Testing across multiple donors is essential for robust conclusions.

Given heterogeneity in the single-KO phenotypes, we tested whether dual KO of ID3 and SOX4 improves CAR T effector function using xenograft mouse models. Mice treated with dual-KO CAR T cells exhibited delayed tumor relapse compared to single-KO and WT CAR T cells, suggesting a cooperative role for SOX4 and ID3 in regulating long-term responses. This supports findings that targeting multiple transcription factors simultaneously, such as NR4A family members,[30] improves CAR T durability.[74,75] Although NSG mice lack proper host immunity, WT and single-KO CAR T cells were dysfunctional in relapsed tumors, probably due to persistent antigen exposure from the MSLN-expressing tumor cells. Continuous CAR engagement with tumor cells likely leads to early cytotoxic activity, followed by gradual loss of function due to sustained stimulation, ultimately allowing a small reservoir of tumor cells to persist and drive relapse in WT and single-KO-treated animals. In contrast, DKO CAR T cells demonstrated improved control of residual tumors, suggesting enhanced resistance to antigen-driven exhaustion and superior long-term functional persistence. Dissecting the transcriptional and signaling programs of DKO CAR T cells, along with *in vivo* tumor re-challenge studies, will be important next steps to better understand how these factors regulate CAR T cell exhaustion and contribute to long-term antitumor protection.

Lastly, the challenging TME of PDAC likely played a significant role in the limited efficacy of huCART-meso as a monotherapy. Strategies to activate immunity in PDAC are under investigation and hold promise to boost immunotherapy results.[76] Given the ability of huCART-meso cells to infiltrate metastases and persist in peritoneal fluid with an acceptable safety profile, combination strategies could enhance therapeutic outcomes. Potential approaches include co-administration with checkpoint inhibitors targeting the programmed cell death 1 (PD-1)/programmed death-ligand 1 (PD-L1) axis or blocking immunosuppressive tumor-derived factors such as transforming growth factor

(E) UMAP projection of scRNA-seq data from recurrent TILs harvested from mice injected with WT CAR T cells (ND561, $n = 1$ donor) and SOX4-KO CAR T cells (ND561 and ND539, $n = 2$ donors).
(F) UMAP projection with broad T cell subsets labeled. NK-like T cells clustered on the left (cluster 2) and all other clusters were defined as GZMK$^+$ exhausted T cells (Tex), right.
(G) huCART-meso expression in recurrent tumor TILs.
(H) Cluster distribution depicting the frequency that WT and SOX4KO-injected recurrent tumor TILs were found within the broad clusters defined in (F). *y* axis represents the percent of cells found within each cell type cluster for each condition (WT or SOX4KO). The percent was calculated by taking the number of cells per condition within each cell type cluster and dividing by the total number of cells in that condition. SOX4KO condition was averaged for the two mice and visualized via bar plot, and circles depict the individual values for each mouse; moderated t test using the propeller method.
(I) Gene expression levels of TNFRSF9, TIGIT, LAG3, and HAVCR2 in recurrent tumor CARpos TILs extracted from mice injected with WT and SOX4KO CAR T cells.
****$p < 0.0001$, ***$p < 0.001$, ns: not significant. See also Figure S4.

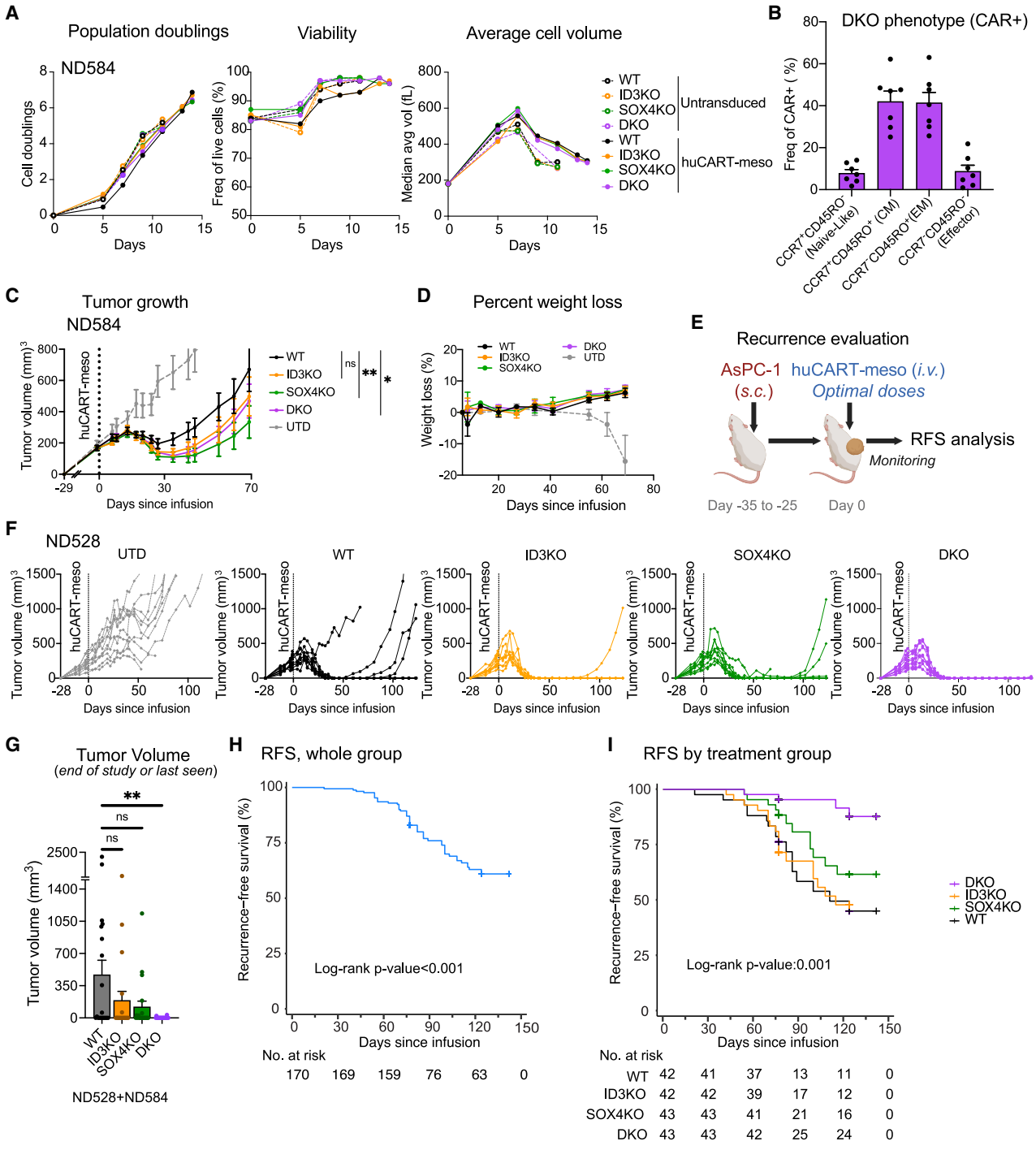


Figure 5. Double KO of SOX4 and ID3 in huCART-meso cells provides sustained protection against tumor recurrence

(A) Population doublings, viability, and average cell volume of ND584 WT, ID3KO, SOX4KO, and DKO huCART-meso (solid lines) and un-transduced cells (UTD) (dashed lines).

(B) Post-expansion phenotype characterization using flow cytometry of huCART-meso DKO cells derived from healthy donors; mean ± SEM. Each dot represents one donor, $n = 7$.

(C) Tumor growth volumes of AsPC-1 tumor-bearing mice treated with suboptimal doses of UTD ($n = 8$ mice), WT, ID3KO, SOX4KO, or DKO ND584 huCART-meso cells (5×10^5 CAR T cells/mouse, $n = 12$ mice per group); two-Way ANOVA with Geisser-Greenhouse correction and Dunnett's post hoc test; mean ± SEM. Dashed line indicates the day of huCART infusion (day 0).

(D) Percentage of weight loss of mice shown in (C), mean ± SEM.

(legend continued on next page)

Table 4. Relapse-free survival

Characteristic	*N*	Event *N*	Median survival
Overall	170	51	NR (NE, NE)
Treatment			
WT	42	17	111 (86, NE)
ID3KO	42	18	115 (100, NE)
SOX4KO	43	12	NR (100, NE)
DKO	43	4	NR (NE, NE)

N, total number of mice; Event *N*, total number of events (recurrence, death, or censored); WT, wild type; DKO, double knockout; NR, not reached; NE, not estimable.

β.[25,77,78] Preclinical and early-phase clinical studies have shown improved CAR T cell efficacy with such combination therapies.[79] Additionally, targeting tumor stroma to enhance CAR T cell extravasation and modulating myeloid compartments via CD40/CD40L targeting could improve antitumor activity.[80–83]

In conclusion, this study provides important insights into the challenges of CAR T cell therapy for PDAC. While huCART-meso therapy demonstrated a favorable safety profile, its efficacy was limited by poor persistence and low huCART-meso tumor infiltration. Future strategies, including combination therapies and transcription factor modulation, hold promise for enhancing CAR T cell function in solid tumors. Continued research in these areas will be essential to unlocking the full therapeutic potential of cell-based immunotherapies for PDAC.

Limitations of the study

Limited sample availability, small patient cohorts, and variability in prior treatments challenge definitive conclusions for certain aspects of our investigation.

We focused on uncovering the intrinsic mechanisms driving CAR T cell exhaustion using subcutaneous xenograft models, which provide a controlled platform for assessing CAR T cell dynamics but do not fully mimic the pancreatic TME. The use of immunocompromised mice also limits the evaluation of interactions with endogenous immune cells. Future studies using orthotopic syngeneic models and tumor re-challenge experiments will be important to further validate the long-term efficacy and durability of DKO CAR T cells in more physiological settings. Despite these constraints, our *in vivo* assays provide valuable insights into the efficacy and persistence of gene-edited CAR T cells.

RESOURCE AVAILABILITY

Lead contact

Further information and requests for resources and reagents should be directed to and will be fulfilled by the lead contact, Dr. Carl H. June (cjune@upenn.edu).

Materials availability

The CAR construct will be available under a material transfer agreement upon request. The sgRNAs and primer sequences are listed in Table S3. The anti-huCART-MSLN anti-idiotype antibody was generously provided by Novartis.

Data and code availability

- Single-cell RNA-sequencing data generated in this study are available through GEO. The accession number is listed in the deposited data section of the key resources table.
- This paper does not report original code. Seurat was used to analyze scRNA-seq data; see STAR Methods for details.
- Any additional information required to reanalyze the data reported in this paper is available from the lead contact upon request.

ACKNOWLEDGMENTS

We thank patients and their families for participating in this clinical trial. We thank the CCI Clinical Trials Unit; Clinical Operations, Monitoring, and Safety Teams; the Hospital of the University of Pennsylvania Apheresis Unit for PBMC collections; the Clinical Cell and Vaccine Production Facility; the Translational and Correlative Studies Laboratory; and the Product Development Lab from Penn CCI. We acknowledge the Human Immunology Core at Penn for providing human T cells. Immunohistochemistry and slide imaging have been provided by the Penn Vet Comparative Pathology Core (RRID: SCR_022438), which is partially supported by the University of Pennsylvania Abramson Cancer Center Support Grant from the NIH (P30 CA016520). The Aperio Versa 200 scanner for slide imaging and analysis was supported by an NIH Shared Instrumentation Grant (S10 OD023465-01A1). The Leica BOND RXm was acquired through the Penn Vet IIZD Core pilot grant.

Research was supported by a SU2C-Lustgarten Foundation Translational Cancer Research Team Grant, grant numbers SU2C-AACR-DT21-17 and SU2C-RT6162. S.L.B. is supported by NIH grant CA263922. C.R.G. is supported by the National Cancer Institute NIH grant R50CA305050 and American Cancer Society Post-doctoral Fellowship PF-19-202-01-DMC. W.-T.H., R.M.Y., and C.H.J. are supported by NIH grant P01CA214278. C.H.J., R.M.Y., and M.A.A. are supported by the Parker Institute for Cancer Immunotherapy Project Award-CJ13. Schematics were generated using BioRender.com.

(E) Experimental design for relapse analyses in AsPC-1 tumor-bearing xenografts treated with curative doses of WT, ID3KO, SOX4KO, and DKO huCART-meso cells (1×10^6 CAR T cells/mouse).
(F) Individual tumor volumes of mice cured with ND528 UTD, WT, ID3KO, SOX4KO, and DKO huCART-meso cells until 4 months after infusion (day 123).
(G) Individual tumor volumes of mice treated with curative doses of ND528 and ND584 WT, ID3KO, SOX4KO, and DKO huCART-meso cells at the end of the study or last seen, whatever comes first; Kruskal-Wallis plus Dunn's test (mean ± SEM).
(H) Relapse-free survival (RFS) plot for mice treated with WT, ID3KO, SOX4KO, or DKO huCART-meso cells. Plot represents RFS of all groups combined (ND528 + ND584, $n = 170$ mice). Multiple independent experiments were performed.
(I) RFS analysis by treatment group. Based on Kaplan-Meier method, median RFS for the WT group ($n = 42$) was 111 days (95% confidence interval [CI]: 86, NE), and ID3KO group ($n = 42$) had a median RFS of 115 (95% CI: 100, NE) days. The median survival time for the SOX4KO ($n = 43$) and DKO ($n = 43$) group was not reached (the estimated survival curve did not fall below 0.5 by the data cutoff time). Subjects at risk refer to the number of mice in the study being monitored at each time point and that have not yet experienced relapse, recurrence, or death. Latest endpoint day for some of the studies in the combined analysis of (H) and (I) was day 141 post infusion. NE, not estimable.
$^{**}p < 0.01$,$^{*}p < 0.05$, ns: not significant. See also Figure S5.

AUTHOR CONTRIBUTIONS

M.A.A. and C.R.G. designed, conducted, and analyzed experiments and wrote the manuscript. J.S.B.-R. analyzed data and co-wrote the manuscript. S.A., D. G., A.K.R., and S.K. assisted with experiments. S.A. and A.J.R. assisted with assays, analysis, and manuscript editing. A.W. and W.-T.H. performed RFS analyses. H.H., W.W., K.M.G., and G.D. assisted with bioinformatics. Z.Z. assisted with genomics assays. V.E.G. and E.O.H. contributed to resources, funding, investigation, and administration. J.T., A.H., D.A.T., and G.N. contributed to investigation. E.D., G.P., A.B., D.L.S., J.K.J., and J.A.F. contributed to investigation, methodology, and administration. C.H.J., S.L.B., R.M.Y., and M. H.O. led conceptualization, design, interpretation, analysis, and manuscript preparation.

DECLARATION OF INTERESTS

J.K.J. consults for BlueWhale Bio. A.J.R. consults for Affini-T Therapeutics. C. H.J. is an inventor on patents related to CAR therapy products and may receive a portion of royalties from Kite to the University of Pennsylvania. J.A.F. receives funding from Tmunity Therapeutics and Danaher Corporation, consults for Retro Biosciences, and serves on the Scientific Advisory Boards for Cartography Bio and Shennon Biotechnologies, Inc. C.H.J. is a scientific co-founder and holds equity in Capstan Therapeutics, Dispatch Biotherapeutics, and BlueWhale Bio; serves on the board of AC Immune; and is a scientific advisor to BlueSphere Bio, Cabaletta, Carisma, Cartography, Cellares, CellCarta, Celldex, Danaher, Decheng, ImmuneSensor, Kite Pharma, Poseida, Verismo, Viracta, ViTToria, and WIRB-Copernicus Group. C.H.J. and R.M.Y. are inventors on patents and/or patent applications licensed to Novartis and Kite Pharma and may receive revenue from them. M.H.O. is a consultant for Alligator and Merus and received funding from BMS, Akamis, Genmab, Geistlich, Arcus, Celldex, Elicio, and Revolution Medicine.

DECLARATION OF GENERATIVE AI AND AI-ASSISTED TECHNOLOGIES IN THE WRITING PROCESS

M.A.A. and C.R.G. used AI-assisted resources during the manuscript preparation to improve text clarity and writing efficiency. After using this tool, the authors thoroughly reviewed and edited the content as needed and take full responsibility for the content of the publication.

STAR★METHODS

Detailed methods are provided in the online version of this paper and include the following:

- KEY RESOURCES TABLE
- EXPERIMENTAL MODEL AND STUDY PARTICIPANT DETAILS
  - Study participants
  - Cell lines
  - Mice
  - Primary human T lymphocytes from healthy donors
- METHOD DETAILS
  - Lentiviral vector production
  - Transduction of CAR-redirected human T cells
  - Flow cytometry and sorting
  - Clinical trial design
  - Clinical Cell manufacture
  - Quantitative PCR analysis of clinical samples
  - Serum cytokine profiling
  - Production of human CRISPR-Engineered CAR-T cells
  - Mouse experiments
  - Standard immunohistochemistry (IHC) analyses
  - Single-cell RNA-seq library preparation
  - Single-cell RNA-seq analysis
- QUANTIFICATION AND STATISTICAL ANALYSIS

SUPPLEMENTAL INFORMATION

Supplemental information can be found online at https://doi.org/10.1016/j.xcrm.2025.102301.

Received: November 15, 2024
Revised: May 29, 2025
Accepted: July 23, 2025
Published: August 18, 2025

REFERENCES

1. Park, W., Chawla, A., and O'Reilly, E.M. (2021). Pancreatic Cancer: A Review. JAMA *326*, 851–862. https://doi.org/10.1001/jama.2021.13027.
2. Conroy, T., Desseigne, F., Ychou, M., Bouché, O., Guimbaud, R., Bécouarn, Y., Adenis, A., Raoul, J.L., Gourgou-Bourgade, S., de la Fouchardière, C., et al. (2011). FOLFIRINOX versus gemcitabine for metastatic pancreatic cancer. N. Engl. J. Med. *364*, 1817–1825. https://doi.org/10.1056/NEJMoa1011923.
3. Von Hoff, D.D., Ervin, T., Arena, F.P., Chiorean, E.G., Infante, J., Moore, M., Seay, T., Tjulandin, S.A., Ma, W.W., Saleh, M.N., et al. (2013). Increased survival in pancreatic cancer with nab-paclitaxel plus gemcitabine. N. Engl. J. Med. *369*, 1691–1703. https://doi.org/10.1056/NEJMoa1304369.
4. Topalian, S.L., Hodi, F.S., Brahmer, J.R., Gettinger, S.N., Smith, D.C., McDermott, D.F., Powderly, J.D., Carvajal, R.D., Sosman, J.A., Atkins, M.B., et al. (2012). Safety, activity, and immune correlates of anti-PD-1 antibody in cancer. N. Engl. J. Med. *366*, 2443–2454. https://doi.org/10.1056/NEJMoa1200690.
5. Brahmer, J.R., Tykodi, S.S., Chow, L.Q.M., Hwu, W.J., Topalian, S.L., Hwu, P., Drake, C.G., Camacho, L.H., Kauh, J., Odunsi, K., et al. (2012). Safety and activity of anti-PD-L1 antibody in patients with advanced cancer. N. Engl. J. Med. *366*, 2455–2465. https://doi.org/10.1056/NEJMoa1200694.
6. Royal, R.E., Levy, C., Turner, K., Mathur, A., Hughes, M., Kammula, U.S., Sherry, R.M., Topalian, S.L., Yang, J.C., Lowy, I., and Rosenberg, S.A. (2010). Phase 2 trial of single agent Ipilimumab (anti-CTLA-4) for locally advanced or metastatic pancreatic adenocarcinoma. J. Immunother. *33*, 828–833. https://doi.org/10.1097/CJI.0b013e3181eec14c.
7. Boyiadzis, M.M., Dhodapkar, M.V., Brentjens, R.J., Kochenderfer, J.N., Neelapu, S.S., Maus, M.V., Porter, D.L., Maloney, D.G., Grupp, S.A., Mackall, C.L., et al. (2018). Chimeric antigen receptor (CAR) T therapies for the treatment of hematologic malignancies: clinical perspective and significance. J. Immunother. Cancer *6*, 137. https://doi.org/10.1186/s40425-018-0460-5.
8. June, C.H., and Sadelain, M. (2018). Chimeric Antigen Receptor Therapy. N. Engl. J. Med. *379*, 64–73. https://doi.org/10.1056/NEJMra1706169.
9. Scales, S.J., Gupta, N., Pacheco, G., Firestein, R., French, D.M., Koeppen, H., Rangell, L., Barry-Hamilton, V., Luis, E., Chuh, J., et al. (2014). An antimesothelin-monomethyl auristatin e conjugate with potent antitumor activity in ovarian, pancreatic, and mesothelioma models. Mol. Cancer Ther. *13*, 2630–2640. https://doi.org/10.1158/1535-7163.MCT-14-0487-T.
10. Shimizu, A., Hirono, S., Tani, M., Kawai, M., Okada, K.I., Miyazawa, M., Kitahata, Y., Nakamura, Y., Noda, T., Yokoyama, S., and Yamaue, H. (2012). Coexpression of MUC16 and mesothelin is related to the invasion process in pancreatic ductal adenocarcinoma. Cancer Sci. *103*, 739–746. https://doi.org/10.1111/j.1349-7006.2012.02214.x.
11. Swierczynski, S.L., Maitra, A., Abraham, S.C., Iacobuzio-Donahue, C.A., Ashfaq, R., Cameron, J.L., Schulick, R.D., Yeo, C.J., Rahman, A., Hinkle, D.A., et al. (2004). Analysis of novel tumor markers in pancreatic and biliary carcinomas using tissue microarrays. Hum. Pathol. *35*, 357–366. https://doi.org/10.1016/j.humpath.2003.10.012.

12. Argani, P., Iacobuzio-Donahue, C., Ryu, B., Rosty, C., Goggins, M., Wilentz, R.E., Murugesan, S.R., Leach, S.D., Jaffee, E., Yeo, C.J., et al. (2001). Mesothelin is overexpressed in the vast majority of ductal adenocarcinomas of the pancreas: identification of a new pancreatic cancer marker by serial analysis of gene expression (SAGE). Clin. Cancer Res. *7*, 3862–3868.

13. Winter, J.M., Tang, L.H., Klimstra, D.S., Brennan, M.F., Brody, J.R., Rocha, F.G., Jia, X., Qin, L.X., D'Angelica, M.I., DeMatteo, R.P., et al. (2012). A novel survival-based tissue microarray of pancreatic cancer validates MUC1 and mesothelin as biomarkers. PLoS One *7*, e40157. https://doi.org/10.1371/journal.pone.0040157.

14. Bharadwaj, U., Li, M., Chen, C., and Yao, Q. (2008). Mesothelin-induced pancreatic cancer cell proliferation involves alteration of cyclin E via activation of signal transducer and activator of transcription protein 3. Mol. Cancer Res. *6*, 1755–1765. https://doi.org/10.1158/1541-7786.MCR-08-0095.

15. Li, M., Bharadwaj, U., Zhang, R., Zhang, S., Mu, H., Fisher, W.E., Brunicardi, F.C., Chen, C., and Yao, Q. (2008). Mesothelin is a malignant factor and therapeutic vaccine target for pancreatic cancer. Mol. Cancer Ther. *7*, 286–296. https://doi.org/10.1158/1535-7163.MCT-07-0483.

16. Beatty, G.L., O'Hara, M.H., Lacey, S.F., Torigian, D.A., Nazimuddin, F., Chen, F., Kulikovskaya, I.M., Soulen, M.C., McGarvey, M., Nelson, A.M., et al. (2018). Activity of Mesothelin-Specific Chimeric Antigen Receptor T Cells Against Pancreatic Carcinoma Metastases in a Phase 1 Trial. Gastroenterology *155*, 29–32. https://doi.org/10.1053/j.gastro.2018.03.029.

17. Haas, A.R., Tanyi, J.L., O'Hara, M.H., Gladney, W.L., Lacey, S.F., Torigian, D.A., Soulen, M.C., Tian, L., McGarvey, M., Nelson, A.M., et al. (2019). Phase I Study of Lentiviral-Transduced Chimeric Antigen Receptor-Modified T Cells Recognizing Mesothelin in Advanced Solid Cancers. Mol. Ther. *27*, 1919–1929. https://doi.org/10.1016/j.ymthe.2019.07.015.

18. Albelda, S.M. (2024). CAR T cell therapy for patients with solid tumours: key lessons to learn and unlearn. Nat. Rev. Clin. Oncol. *21*, 47–66. https://doi.org/10.1038/s41571-023-00832-4.

19. Satpathy, A.T., Granja, J.M., Yost, K.E., Qi, Y., Meschi, F., McDermott, G.P., Olsen, B.N., Mumbach, M.R., Pierce, S.E., Corces, M.R., et al. (2019). Massively parallel single-cell chromatin landscapes of human immune cell development and intratumoral T cell exhaustion. Nat. Biotechnol. *37*, 925–936. https://doi.org/10.1038/s41587-019-0206-z.

20. McLane, L.M., Abdel-Hakeem, M.S., and Wherry, E.J. (2019). CD8 T Cell Exhaustion During Chronic Viral Infection and Cancer. Annu. Rev. Immunol. *37*, 457–495. https://doi.org/10.1146/annurev-immunol-041015-055318.

21. Pauken, K.E., Sammons, M.A., Odorizzi, P.M., Manne, S., Godec, J., Khan, O., Drake, A.M., Chen, Z., Sen, D.R., Kurachi, M., et al. (2016). Epigenetic stability of exhausted T cells limits durability of reinvigoration by PD-1 blockade. Science *354*, 1160–1165. https://doi.org/10.1126/science.aaf2807.

22. Vigano, S., Bobisse, S., Coukos, G., Perreau, M., and Harari, A. (2020). Cancer and HIV-1 Infection: Patterns of Chronic Antigen Exposure. Front. Immunol. *11*, 1350. https://doi.org/10.3389/fimmu.2020.01350.

23. Pauken, K.E., and Wherry, E.J. (2015). Overcoming T cell exhaustion in infection and cancer. Trends Immunol. *36*, 265–276. https://doi.org/10.1016/j.it.2015.02.008.

24. Fraietta, J.A., Lacey, S.F., Orlando, E.J., Pruteanu-Malinici, I., Gohil, M., Lundh, S., Boesteanu, A.C., Wang, Y., O'Connor, R.S., Hwang, W.T., et al. (2018). Determinants of response and resistance to CD19 chimeric antigen receptor (CAR) T cell therapy of chronic lymphocytic leukemia. Nat. Med. *24*, 563–571. https://doi.org/10.1038/s41591-018-0010-1.

25. Cherkassky, L., Morello, A., Villena-Vargas, J., Feng, Y., Dimitrov, D.S., Jones, D.R., Sadelain, M., and Adusumilli, P.S. (2016). Human CAR T cells with cell-intrinsic PD-1 checkpoint blockade resist tumor-mediated inhibition. J. Clin. Investig. *126*, 3130–3144. https://doi.org/10.1172/JCI83092.

26. Good, C.R., Aznar, M.A., Kuramitsu, S., Samareh, P., Agarwal, S., Donahue, G., Ishiyama, K., Wellhausen, N., Rennels, A.K., Ma, Y., et al. (2021). An NK-like CAR T cell transition in CAR T cell dysfunction. Cell *184*, 6081–6100.e26. https://doi.org/10.1016/j.cell.2021.11.016.

27. Schuster, S.J., Bishop, M.R., Tam, C.S., Waller, E.K., Borchmann, P., McGuirk, J.P., Jäger, U., Jaglowski, S., Andreadis, C., Westin, J.R., et al. (2019). Tisagenlecleucel in Adult Relapsed or Refractory Diffuse Large B-Cell Lymphoma. N. Engl. J. Med. *380*, 45–56. https://doi.org/10.1056/NEJMoa1804980.

28. Hou, A.J., Chen, L.C., and Chen, Y.Y. (2021). Navigating CAR-T cells through the solid-tumour microenvironment. Nat. Rev. Drug Discov. *20*, 531–550. https://doi.org/10.1038/s41573-021-00189-2.

29. Seo, H., Chen, J., González-Avalos, E., Samaniego-Castruita, D., Das, A., Wang, Y.H., López-Moyado, I.F., Georges, R.O., Zhang, W., Onodera, A., et al. (2019). TOX and TOX2 transcription factors cooperate with NR4A transcription factors to impose CD8(+) T cell exhaustion. Proc. Natl. Acad. Sci. USA *116*, 12410–12415. https://doi.org/10.1073/pnas.1905675116.

30. Chen, J., López-Moyado, I.F., Seo, H., Lio, C.W.J., Hempleman, L.J., Sekiya, T., Yoshimura, A., Scott-Browne, J.P., and Rao, A. (2019). NR4A transcription factors limit CAR T cell function in solid tumours. Nature *567*, 530–534. https://doi.org/10.1038/s41586-019-0985-x.

31. Liu, X., Wang, Y., Lu, H., Li, J., Yan, X., Xiao, M., Hao, J., Alekseev, A., Khong, H., Chen, T., et al. (2019). Genome-wide analysis identifies NR4A1 as a key mediator of T cell dysfunction. Nature *567*, 525–529. https://doi.org/10.1038/s41586-019-0979-8.

32. Haas, A.R., Golden, R.J., Litzky, L.A., Engels, B., Zhao, L., Xu, F., Taraszka, J.A., Ramones, M., Granda, B., Chang, W.J., et al. (2023). Two cases of severe pulmonary toxicity from highly active mesothelin-directed CAR T cells. Mol. Ther. *31*, 2309–2325. https://doi.org/10.1016/j.ymthe.2023.06.006.

33. Eisenhauer, E.A., Therasse, P., Bogaerts, J., Schwartz, L.H., Sargent, D., Ford, R., Dancey, J., Arbuck, S., Gwyther, S., Mooney, M., et al. (2009). New response evaluation criteria in solid tumours: revised RECIST guideline (version 1.1). Eur. J. Cancer *45*, 228–247. https://doi.org/10.1016/j.ejca.2008.10.026.

34. Weber, E.W., Parker, K.R., Sotillo, E., Lynn, R.C., Anbunathan, H., Lattin, J., Good, Z., Belk, J.A., Daniel, B., Klysz, D., et al. (2021). Transient rest restores functionality in exhausted CAR-T cells through epigenetic remodeling. Science *372*, eaba1786. https://doi.org/10.1126/science.aba1786.

35. Guo, X., Zhang, Y., Zheng, L., Zheng, C., Song, J., Zhang, Q., Kang, B., Liu, Z., Jin, L., Xing, R., et al. (2018). Global characterization of T cells in non-small-cell lung cancer by single-cell sequencing. Nat. Med. *24*, 978–985. https://doi.org/10.1038/s41591-018-0045-3.

36. Wang, X., Shen, X., Chen, S., Liu, H., Hong, N., Zhong, H., Chen, X., and Jin, W. (2022). Reinvestigation of Classic T Cell Subsets and Identification of Novel Cell Subpopulations by Single-Cell RNA Sequencing. J. Immunol. *208*, 396–406. https://doi.org/10.4049/jimmunol.2100581.

37. Cano-Gamez, E., Soskic, B., Roumeliotis, T.I., So, E., Smyth, D.J., Baldrighi, M., Willé, D., Nakic, N., Esparza-Gordillo, J., Larminie, C.G.C., et al. (2020). Single-cell transcriptomics identifies an effectorness gradient shaping the response of CD4(+) T cells to cytokines. Nat. Commun. *11*, 1801. https://doi.org/10.1038/s41467-020-15543-y.

38. Wang, H., Fu, Y., Da, B.B., and Xiong, G. (2022). Single-Cell Sequencing Identifies the Heterogeneity of CD8+ T Cells and Novel Biomarker Genes in Hepatocellular Carcinoma. J. Healthc. Eng. *2022*, 8256314. https://doi.org/10.1155/2022/8256314.

39. Giles, J.R., Manne, S., Freilich, E., Oldridge, D.A., Baxter, A.E., George, S., Chen, Z., Huang, H., Chilukuri, L., Carberry, M., et al. (2022). Human epigenetic and transcriptional T cell differentiation atlas for identifying functional T cell-specific enhancers. Immunity *55*, 557–574.e7. https://doi.org/10.1016/j.immuni.2022.02.004.

40. Chen, Y., Shen, J., Kasmani, M.Y., Topchyan, P., and Cui, W. (2021). Single-Cell Transcriptomics Reveals Core Regulatory Programs That

Determine the Heterogeneity of Circulating and Tissue-Resident Memory CD8(+) T Cells. Cells *10*, 2143. https://doi.org/10.3390/cells10082143.

41. Zheng, L., Qin, S., Si, W., Wang, A., Xing, B., Gao, R., Ren, X., Wang, L., Wu, X., Zhang, J., et al. (2021). Pan-cancer single-cell landscape of tumor-infiltrating T cells. Science *374*, abe6474. https://doi.org/10.1126/science.abe6474.

42. Szabo, P.A., Levitin, H.M., Miron, M., Snyder, M.E., Senda, T., Yuan, J., Cheng, Y.L., Bush, E.C., Dogra, P., Thapa, P., et al. (2019). Single-cell transcriptomics of human T cells reveals tissue and activation signatures in health and disease. Nat. Commun. *10*, 4706. https://doi.org/10.1038/s41467-019-12464-3.

43. Li, J., He, Y., Hao, J., Ni, L., and Dong, C. (2018). High Levels of Eomes Promote Exhaustion of Anti-tumor CD8(+) T Cells. Front. Immunol. *9*, 2981. https://doi.org/10.3389/fimmu.2018.02981.

44. Klampatsa, A., Dimou, V., and Albelda, S.M. (2021). Mesothelin-targeted CAR-T cell therapy for solid tumors. Expert Opin. Biol. Ther. *21*, 473–486. https://doi.org/10.1080/14712598.2021.1843628.

45. Katz, S.C., Burga, R.A., McCormack, E., Wang, L.J., Mooring, W., Point, G.R., Khare, P.D., Thorn, M., Ma, Q., Stainken, B.F., et al. (2015). Phase I Hepatic Immunotherapy for Metastases Study of Intra-Arterial Chimeric Antigen Receptor-Modified T-cell Therapy for CEA+ Liver Metastases. Clin. Cancer Res. *21*, 3149–3159. https://doi.org/10.1158/1078-0432.CCR-14-1421.

46. Annunziata, C.M., Ghobadi, A., Pennella, E.J., Vanas, J., Powell, C., Pavelova, M., Wagner, C., Kuo, M., Dansky Ullmann, C., Hassan, R., and Thaker, P.H. (2020). Feasibility and preliminary safety and efficacy of first-in-human intraperitoneal delivery of MCY-M11, anti-human-mesothelin CAR mRNA transfected into peripheral blood mononuclear cells, for ovarian cancer and malignant peritoneal mesothelioma. J. Clin. Oncol. *38*, 3014. https://doi.org/10.1200/JCO.2020.38.15_suppl.3014.

47. Katz, S.C., Moody, A.E., Guha, P., Hardaway, J.C., Prince, E., LaPorte, J., Stancu, M., Slansky, J.E., Jordan, K.R., Schulick, R.D., et al. (2020). HITMSURE: Hepatic immunotherapy for metastases phase Ib anti-CEA CAR-T study utilizing pressure enabled drug delivery. J. Immunother. Cancer *8*, e001097. https://doi.org/10.1136/jitc-2020-001097.

48. Narayan, V., Barber-Rotenberg, J.S., Jung, I.Y., Lacey, S.F., Rech, A.J., Davis, M.M., Hwang, W.T., Lal, P., Carpenter, E.L., Maude, S.L., et al. (2022). PSMA-targeting TGFbeta-insensitive armored CAR T cells in metastatic castration-resistant prostate cancer: a phase 1 trial. Nat. Med. *28*, 724–734. https://doi.org/10.1038/s41591-022-01726-1.

49. Steffin, D., Ghatwai, N., Montalbano, A., Rathi, P., Courtney, A.N., Arnett, A.B., Fleurence, J., Sweidan, R., Wang, T., Zhang, H., et al. (2024). Interleukin-15-armored GPC3-CAR T cells for patients with solid cancers. Preprint at Res. Sq. https://doi.org/10.21203/rs.3.rs-4103623/v1.

50. Wang, Y., Chen, M., Wu, Z., Tong, C., Dai, H., Guo, Y., Liu, Y., Huang, J., Lv, H., Luo, C., et al. (2018). CD133-directed CAR T cells for advanced metastasis malignancies: A phase I trial. OncoImmunology *7*, e1440169. https://doi.org/10.1080/2162402X.2018.1440169.

51. Zhang, Y., Chertov, O., Zhang, J., Hassan, R., and Pastan, I. (2011). Cytotoxic activity of immunotoxin SS1P is modulated by TACE-dependent mesothelin shedding. Cancer Res. *71*, 5915–5922. https://doi.org/10.1158/0008-5472.CAN-11-0466.

52. Li, J., Byrne, K.T., Yan, F., Yamazoe, T., Chen, Z., Baslan, T., Richman, L.P., Lin, J.H., Sun, Y.H., Rech, A.J., et al. (2018). Tumor Cell-Intrinsic Factors Underlie Heterogeneity of Immune Cell Infiltration and Response to Immunotherapy. Immunity *49*, 178–193.e7. https://doi.org/10.1016/j.immuni.2018.06.006.

53. Kim, R.H., Plesa, G., Gladney, W., Kulikovskaya, I., Levine, B.L., Lacey, S.F., June, C.H., Melenhorst, J.J., and Beatty, G.L. (2017). Effect of chimeric antigen receptor (CAR) T cells on clonal expansion of endogenous non-CAR T cells in patients (pts) with advanced solid cancer. J. Clin. Oncol. *35*, 3011. https://doi.org/10.1200/JCO.2017.35.15_suppl.3011.

54. Halbrook, C.J., Lyssiotis, C.A., Pasca di Magliano, M., and Maitra, A. (2023). Pancreatic cancer: Advances and challenges. Cell *186*, 1729–1754. https://doi.org/10.1016/j.cell.2023.02.014.

55. Camviel, N., Wolf, B., Croce, G., Gfeller, D., Zoete, V., and Arber, C. (2022). Both APRIL and antibody-fragment-based CAR T cells for myeloma induce BCMA downmodulation by trogocytosis and internalization. J. Immunother. Cancer *10*, e005091. https://doi.org/10.1136/jitc-2022-005091.

56. Caruso, H.G., Hurton, L.V., Najjar, A., Rushworth, D., Ang, S., Olivares, S., Mi, T., Switzer, K., Singh, H., Huls, H., et al. (2015). Tuning Sensitivity of CAR to EGFR Density Limits Recognition of Normal Tissue While Maintaining Potent Antitumor Activity. Cancer Res. *75*, 3505–3518. https://doi.org/10.1158/0008-5472.CAN-15-0139.

57. Davenport, A.J., Jenkins, M.R., Cross, R.S., Yong, C.S., Prince, H.M., Ritchie, D.S., Trapani, J.A., Kershaw, M.H., Darcy, P.K., and Neeson, P.J. (2015). CAR-T Cells Inflict Sequential Killing of Multiple Tumor Target Cells. Cancer Immunol. Res. *3*, 483–494. https://doi.org/10.1158/2326-6066.CIR-15-0048.

58. Hamieh, M., Dobrin, A., Cabriolu, A., van der Stegen, S.J.C., Giavridis, T., Mansilla-Soto, J., Eyquem, J., Zhao, Z., Whitlock, B.M., Miele, M.M., et al. (2019). CAR T cell trogocytosis and cooperative killing regulate tumour antigen escape. Nature *568*, 112–116. https://doi.org/10.1038/s41586-019-1054-1.

59. Zhai, Y., Du, Y., Li, G., Yu, M., Hu, H., Pan, C., Wang, D., Shi, Z., Yan, X., Li, X., et al. (2023). Trogocytosis of CAR molecule regulates CAR-T cell dysfunction and tumor antigen escape. Signal Transduct. Target. Ther. *8*, 457. https://doi.org/10.1038/s41392-023-01708-w.

60. Jonsson, A.H., Zhang, F., Dunlap, G., Gomez-Rivas, E., Watts, G.F.M., Faust, H.J., Rupani, K.V., Mears, J.R., Meednu, N., Wang, R., et al. (2022). Granzyme K(+) CD8 T cells form a core population in inflamed human tissue. Sci. Transl. Med. *14*, eabo0686. https://doi.org/10.1126/scitranslmed.abo0686.

61. Flemming, A. (2021). GZMK(+) T cells a hallmark of immune ageing. Nat. Rev. Immunol. *21*, 1. https://doi.org/10.1038/s41577-020-00486-8.

62. Mogilenko, D.A., Shpynov, O., Andhey, P.S., Arthur, L., Swain, A., Esaulova, E., Brioschi, S., Shchukina, I., Kerndl, M., Bambouskova, M., et al. (2021). Comprehensive Profiling of an Aging Immune System Reveals Clonal GZMK(+) CD8(+) T Cells as Conserved Hallmark of Inflammaging. Immunity *54*, 99–115.e12. https://doi.org/10.1016/j.immuni.2020.11.005.

63. Good, Z., Spiegel, J.Y., Sahaf, B., Malipatlolla, M.B., Ehlinger, Z.J., Kurra, S., Desai, M.H., Reynolds, W.D., Wong Lin, A., Vandris, P., et al. (2022). Post-infusion CAR T(Reg) cells identify patients resistant to CD19-CAR therapy. Nat. Med. *28*, 1860–1871. https://doi.org/10.1038/s41591-022-01960-7.

64. Haradhvala, N.J., Leick, M.B., Maurer, K., Gohil, S.H., Larson, R.C., Yao, N., Gallagher, K.M.E., Katsis, K., Frigault, M.J., Southard, J., et al. (2022). Distinct cellular dynamics associated with response to CAR-T therapy for refractory B cell lymphoma. Nat. Med. *28*, 1848–1859. https://doi.org/10.1038/s41591-022-01959-0.

65. Bachireddy, P., Azizi, E., Burdziak, C., Nguyen, V.N., Ennis, C.S., Maurer, K., Park, C.Y., Choo, Z.N., Li, S., Gohil, S.H., et al. (2021). Mapping the evolution of T cell states during response and resistance to adoptive cellular therapy. Cell Rep. *37*, 109992. https://doi.org/10.1016/j.celrep.2021.109992.

66. Li, H., van der Leun, A.M., Yofe, I., Lubling, Y., Gelbard-Solodkin, D., van Akkooi, A.C.J., van den Braber, M., Rozeman, E.A., Haanen, J.B.A.G., Blank, C.U., et al. (2019). Dysfunctional CD8 T Cells Form a Proliferative, Dynamically Regulated Compartment within Human Melanoma. Cell *176*, 775–789.e18. https://doi.org/10.1016/j.cell.2018.11.043.

67. Lipp, J.J., Wang, L., Yang, H., Yao, F., Harrer, N., Müller, S., Berezowska, S., Dorn, P., Marti, T.M., Schmid, R.A., et al. (2022). Functional and molecular characterization of PD1(+) tumor-infiltrating lymphocytes from lung cancer patients. OncoImmunology *11*, 2019466. https://doi.org/10.1080/2162402X.2021.2019466.

68. Kavyanifar, A., Turan, S., and Lie, D.C. (2018). SoxC transcription factors: multifunctional regulators of neurodevelopment. Cell Tissue Res. *371*, 91–103. https://doi.org/10.1007/s00441-017-2708-7.

69. Fraidenraich, D., Stillwell, E., Romero, E., Wilkes, D., Manova, K., Basson, C.T., and Benezra, R. (2004). Rescue of cardiac defects in id knockout embryos by injection of embryonic stem cells. Science *306*, 247–252. https://doi.org/10.1126/science.1102612.

70. Kontarakis, Z., and Stainier, D.Y.R. (2020). Genetics in Light of Transcriptional Adaptation. Trends Genet. *36*, 926–935. https://doi.org/10.1016/j.tig.2020.08.008.

71. Brodin, P., and Davis, M.M. (2017). Human immune system variation. Nat. Rev. Immunol. *17*, 21–29. https://doi.org/10.1038/nri.2016.125.

72. Brodin, P., Jojic, V., Gao, T., Bhattacharya, S., Angel, C.J.L., Furman, D., Shen-Orr, S., Dekker, C.L., Swan, G.E., Butte, A.J., et al. (2015). Variation in the human immune system is largely driven by non-heritable influences. Cell *160*, 37–47. https://doi.org/10.1016/j.cell.2014.12.020.

73. Bai, Z., Feng, B., McClory, S.E., de Oliveira, B.C., Diorio, C., Gregoire, C., Tao, B., Yang, L., Zhao, Z., Peng, L., et al. (2024). Single-cell CAR T atlas reveals type 2 function in 8-year leukaemia remission. Nature *634*, 702–711. https://doi.org/10.1038/s41586-024-07762-w.

74. Jung, I.Y., Narayan, V., McDonald, S., Rech, A.J., Bartoszek, R., Hong, G., Davis, M.M., Xu, J., Boesteanu, A.C., Barber-Rotenberg, J.S., et al. (2022). BLIMP1 and NR4A3 transcription factors reciprocally regulate antitumor CAR T cell stemness and exhaustion. Sci. Transl. Med. *14*, eabn7336. https://doi.org/10.1126/scitranslmed.abn7336.

75. Pal, S.K., Tran, B., Haanen, J.B.A.G., Hurwitz, M.E., Sacher, A., Tannir, N.M., Budde, L.E., Harrison, S.J., Klobuch, S., Patel, S.S., et al. (2024). CD70-Targeted Allogeneic CAR T-Cell Therapy for Advanced Clear Cell Renal Cell Carcinoma. Cancer Discov. *14*, 1176–1189. https://doi.org/10.1158/2159-8290.CD-24-0102.

76. Vonderheide, R.H. (2020). CD40 Agonist Antibodies in Cancer Immunotherapy. Annu. Rev. Med. *71*, 47–58. https://doi.org/10.1146/annurev-med-062518-045435.

77. Bayne, L.J., Beatty, G.L., Jhala, N., Clark, C.E., Rhim, A.D., Stanger, B.Z., and Vonderheide, R.H. (2012). Tumor-derived granulocyte-macrophage colony-stimulating factor regulates myeloid inflammation and T cell immunity in pancreatic cancer. Cancer Cell *21*, 822–835. https://doi.org/10.1016/j.ccr.2012.04.025.

78. Soares, K.C., Rucki, A.A., Kim, V., Foley, K., Solt, S., Wolfgang, C.L., Jaffee, E.M., and Zheng, L. (2015). TGF-beta blockade depletes T regulatory cells from metastatic pancreatic tumors in a vaccine dependent manner. Oncotarget *6*, 43005–43015. https://doi.org/10.18632/oncotarget.5656.

79. Adusumilli, P.S., Zauderer, M.G., Rivière, I., Solomon, S.B., Rusch, V.W., O'Cearbhaill, R.E., Zhu, A., Cheema, W., Chintala, N.K., Halton, E., et al. (2021). A Phase I Trial of Regional Mesothelin-Targeted CAR T-cell Therapy in Patients with Malignant Pleural Disease, in Combination with the Anti-PD-1 Agent Pembrolizumab. Cancer Discov. *11*, 2748–2763. https://doi.org/10.1158/2159-8290.CD-21-0407.

80. Kuhn, N.F., Purdon, T.J., van Leeuwen, D.G., Lopez, A.V., Curran, K.J., Daniyan, A.F., and Brentjens, R.J. (2019). CD40 Ligand-Modified Chimeric Antigen Receptor T Cells Enhance Antitumor Function by Eliciting an Endogenous Antitumor Response. Cancer Cell *35*, 473–488.e6. https://doi.org/10.1016/j.ccell.2019.02.006.

81. Wehrli, M., Guinn, S., Birocchi, F., Kuo, A., Sun, Y., Larson, R.C., Almazan, A.J., Scarfò, I., Bouffard, A.A., Bailey, S.R., et al. (2024). Mesothelin CAR T-cells secreting anti-FAP/anti-CD3 molecules efficiently target pancreatic adenocarcinoma and its stroma. Clin. Cancer Res. *30*, 1859–1877. https://doi.org/10.1158/1078-0432.CCR-23-3841.

82. Xiao, Z., Todd, L., Huang, L., Noguera-Ortega, E., Lu, Z., Huang, L., Kopp, M., Li, Y., Pattada, N., Zhong, W., et al. (2023). Desmoplastic stroma restricts T cell extravasation and mediates immune exclusion and immunosuppression in solid tumors. Nat. Commun. *14*, 5110. https://doi.org/10.1038/s41467-023-40850-5.

83. Zhang, Y., Wang, P., Wang, T., Fang, Y., Ding, Y., and Qian, Q. (2021). Chimeric antigen receptor T cells engineered to secrete CD40 agonist antibodies enhance antitumor efficacy. J. Transl. Med. *19*, 82. https://doi.org/10.1186/s12967-021-02750-4.

84. Phipson, B., Sim, C.B., Porrello, E.R., Hewitt, A.W., Powell, J., and Oshlack, A. (2022). propeller: testing for differences in cell type proportions in single cell data. Bioinformatics *38*, 4720–4726. https://doi.org/10.1093/bioinformatics/btac582.

85. Butler, A., Hoffman, P., Smibert, P., Papalexi, E., and Satija, R. (2018). Integrating single-cell transcriptomic data across different conditions, technologies, and species. Nat. Biotechnol. *36*, 411–420. https://doi.org/10.1038/nbt.4096.

86. Stuart, T., Butler, A., Hoffman, P., Hafemeister, C., Papalexi, E., Mauck, W.M., 3rd, Hao, Y., Stoeckius, M., Smibert, P., and Satija, R. (2019). Comprehensive Integration of Single-Cell Data. Cell *177*, 1888–1902. e21. https://doi.org/10.1016/j.cell.2019.05.031.

87. Hafemeister, C., and Satija, R. (2019). Normalization and variance stabilization of single-cell RNA-seq data using regularized negative binomial regression. Genome Biol. *20*, 296. https://doi.org/10.1186/s13059-019-1874-1.

88. Kutner, R.H., Zhang, X.Y., and Reiser, J. (2009). Production, concentration and titration of pseudotyped HIV-1-based lentiviral vectors. Nat. Protoc. *4*, 495–505. https://doi.org/10.1038/nprot.2009.22.

89. Carpenito, C., Milone, M.C., Hassan, R., Simonet, J.C., Lakhal, M., Suhoski, M.M., Varela-Rohena, A., Haines, K.M., Heitjan, D.F., Albelda, S.M., et al. (2009). Control of large, established tumor xenografts with genetically retargeted human T cells containing CD28 and CD137 domains. Proc. Natl. Acad. Sci. USA *106*, 3360–3365. https://doi.org/10.1073/pnas.0813101106.

90. Porter, D.L., Kalos, M., Zheng, Z., Levine, B., and June, C. (2011). Chimeric Antigen Receptor Therapy for B-cell Malignancies. J. Cancer *2*, 331–332. https://doi.org/10.7150/jca.2.331.

91. Teachey, D.T., Lacey, S.F., Shaw, P.A., Melenhorst, J.J., Maude, S.L., Frey, N., Pequignot, E., Gonzalez, V.E., Chen, F., Finklestein, J., et al. (2016). Identification of Predictive Biomarkers for Cytokine Release Syndrome after Chimeric Antigen Receptor T-cell Therapy for Acute Lymphoblastic Leukemia. Cancer Discov. *6*, 664–679. https://doi.org/10.1158/2159-8290.CD-16-0040.

92. Agarwal, S., Wellhausen, N., Levine, B.L., and June, C.H. (2021). Production of Human CRISPR-Engineered CAR-T Cells. J. Vis. Exp. *169*, e62299. https://doi.org/10.3791/62299.

93. Linderman, G.C., Zhao, J., Roulis, M., Bielecki, P., Flavell, R.A., Nadler, B., and Kluger, Y. (2022). Zero-preserving imputation of single-cell RNA-seq data. Nat. Commun. *13*, 192. https://doi.org/10.1038/s41467-021-27729-z.

STAR★METHODS

KEY RESOURCES TABLE

REAGENT or RESOURCE	SOURCE	IDENTIFIER
Antibodies		
anti-human CD3	Biolegend	Cat# 317322; RRID:AB_2561911
anti-human CD3	Biolegend	Cat# 317308; RRID:AB_571913
anti-human CD4	Biolegend	Cat# 357412; RRID:AB_2565664
anti-human CD4	Biolegend	Cat# 317440; RRID:AB_2562912
anti-human CD4	Biolegend	Cat# 317428; RRID:AB_1186122
anti-human CD8	BD Pharmingen	Cat# 560179; RRID:AB_1645481
anti-human CD8	Biolegend	Cat# 344748; RRID:AB_2629584
anti-human CD14	Biolegend	Cat# 301838; RRID:AB_2562909
anti-human CD45	Biolegend	Cat# 304032; RRID:AB_2561357
anti-human CD45	Biolegend	Cat# 304017; RRID:AB_389314
anti-human CD45	Biolegend	Cat# 304028; RRID:AB_893338
anti-human CD56	Biolegend	Cat# 304608; RRID:AB_314450
anti-human EpCAM	Biolegend	Cat# 324226; RRID:AB_2562735
anti-human EpCAM	Biolegend	Cat# 324238; RRID:AB_2632937
anti-human CD235a	Biolegend	Cat# 349104; RRID:AB_10613463
anti-human Mesothelin	Biolegend	Cat# 530203; RRID:AB_2571909
anti-human CD45RO	Biolegend	Cat# 304244; RRID:AB_2564160
anti-human CCR7	BD Pharmingen	Cat# 561271; RRID:AB_10561679
anti-human IgG F(ab')2	Jackson ImmunoResearch	Cat# 109-066-006; RRID:AB_2337634
TruStain FcX™ PLUS (anti-mouse CD16/32) Antibody	Biolegend	Cat# 156604; RRID:AB_2783138
Human TruStain FcX™ (Fc Receptor Blocking Solution)	Biolegend	Cat# 422302; RRID:AB_2818986
Anti-human CD45 (CD45-LCA)	Cell Signaling Technology	Cat# 13917; RRID:AB_2750898
Biotinylated goat anti-human IgG F(ab')2	Jackson ImmunoResearch	Cat# 109-066-006; RRID:AB_2337634
Bacterial and virus strains		
One Shot™ Stbl3™ Chemically Competent E. coli	Invitrogen	C7373-03
Biological samples		
T lymphocytes from human healthy donors	UPenn Human Immunology Core	N/A
Peritoneal fluid	CCI Clinical Trials Unit/Translational and Correlative Studies Laboratory	N/A
Tumor biopsies (Fine needle aspirates)	CCI Clinical Trials Unit/Translational and Correlative Studies Laboratory	N/A
Blood	CCI Clinical Trials Unit/Translational and Correlative Studies Laboratory	N/A
Chemicals, peptides, and recombinant proteins		
Live/Dead Aqua	ThermoFisher	Cat# L34957
Zombie NIR (Biolegend) Fixable Viability Kits	Biolegend	Cat# 423106
Ficoll® Paque Plus	Millipore	Cat# GE17-1440-0
Alt-R® Cas9 Electroporation Enhancer, 10 nmol	Integrated DNA Technologies	Cat# 1075916
SpyFi Cas9	Aldeveron	Cat# 9214
P3 Primary cell 4D-nucleofactor X Kit L	Lonza	Cat# V4XP-3024
OpTmizer T cell Expansion SFM	Gibco	Cat# A1048501

(*Continued on next page*)

Continued

REAGENT or RESOURCE	SOURCE	IDENTIFIER
Human AB Serum	GeminiBio	Cat#100-512
Recombinant Human IL-7	Peprotech	Cat#200-07
Recombinant Human IL-15	Peprotech	Cat#200-15
DNAse I	Sigma	Cat#10104159001
Lipofectamine 3000	Thermo Fisher Scientific	Cat#L3000015
Matrigel Membrane Matrix	Corning	Cat#356234
Collagenase D	Sigma	Cat# 11088866001
DNase I from bovine pancreas	Sigma	Cat# 11284932001
Ack lysing buffer	Gibco	Cat# A1049201
EDTA (0.5 M), pH 8.0, RNase-free	Thermo Fisher	Cat# AM92 61
BV421 Streptavidin	Biolegend	Cat# 405225
Alexa Fluor 488 Streptavidin	Biolegend	Cat# 405235
APC Streptavidin	Biolegend	Cat# 405235
Critical commercial assays		
NEBNext® Library Quant Kit for Illumina®	New England Biolabs	E7630L
NextSeq 500/550 High Output Kit (75 cycles) v2.5 kit	Illumina	20024906
NextSeq 500/550 High Output Kit v2.5 (150 Cycles)	Illumina	20024907
Chromium Next GEM Single Cell 3′ GEM, Library & Gel Bead Kit v3.1	10X Genomics	1000128
Single Index Kit T Set A	10X Genomics	1000213
Qubit™ dsDNA HS Assay Kit	ThermoFisher	Q32854
BioAnalyzer High Sensitivity DNA Kit	Agilent	5067–4626
DynaBeads CD3x28 (Human)	ThermoFisher	Cat# 11131D
NucleoSpin Gel and PCR Clean-up	Macherey-Nagel	Cat# 74609.50
QIAGEN Plasmid Plus Maxi Kit	QIAGEN	Cat# 12963
EasySep™ Release Human CD45 Positive Selection Kit for Humanized Mice	STEMCELL Technologies	Cat# 100-0140
CountBright Absolute Counting Beads, (ThermoFisher)	Thermo Fisher	Cat# C36950
Milliplex Human 31-plex	Millipore	Cat# SPRCUS707
Milliplex Human 32-Plex	Millipore	Cat# SPRCUS1673
LongAmp™ Taq 2X Master Mix	New England Biolabs	Cat# M0287S
Vacuum Filter/Storage Systems	Corning	Cat# 430770
Deposited data		
Raw and analyzed data	This paper	Database: GEO: GSE276061
Experimental models: Cell lines		
Human (female) HEK293T	ATCC	CRL-11268
Human (female) ASPC-1	ATCC	CRL-1682
Experimental models: Organisms/strains		
NOD/scid/IL2rγ−/− (NSG)	Jackson Laboratory	Cat# 5557
Oligonucleotides		
See Table S3 for sgRNA oligonucleotides and primer sequences		N/A
Recombinant DNA		
pTRPE M5BBz	This paper	N/A
Software and algorithms		
R version 4.2.0	CRAN	https://cran.r-project.org/

(*Continued on next page*)

Continued

REAGENT or RESOURCE	SOURCE	IDENTIFIER
Speckle 1.2.0	(Phipson et al. [84])	https://www.bioconductor.org/packages/release/bioc/html/speckle.html
RStudio 2022.02.2	RStudio Team	http://www.rstudio.com/
Seurat_4.3.0.1	(Butler et al.[85]; Stuart et al. [86])	https://satijalab.org/seurat/
Cell Ranger v3.1.0	10X Genomics	https://www.10xgenomics.com/
sctransform_0.3.5	(Hafemeister and Satija [87])	https://cran.r-project.org/web/packages/sctransform/index.html
SeuratWrappers 0.3.0	(Butler et al.[85]; Stuart et al. [86])	https://satijalab.org/seurat/articles/install.html
Prism v10 Software	GraphPad Software	https://www.graphpad.com/
FlowJo™ v10.8 Software	BD Life Sciences	https://www.flowjo.com
Other		
CRISPick sgRNA designer ([2020])	The Broad Institute	https://portals.broadinstitute.org/gppx/crispick/public
Benchling sgRNA designer tool (https://www.benchling.com, [2020])	Benchling	https://benchling.com/
Synthego's Performance Analysis ICE (short for Inference of CRISPR Edits) tool	Synthego	https://ice.synthego.com/[2021 to 2024]).
BioRender illustration design tool	BioRender	https://biorender.com/

EXPERIMENTAL MODEL AND STUDY PARTICIPANT DETAILS

Study participants

This trial was conducted in accordance with guidelines from the United States Food and Drug Administration (FDA), the International Conference on Harmonization for Good Clinical Practice, the Declaration of Helsinki, and applicable institutional review board (IRB) requirements. The study protocol was approved by the University of Pennsylvania Institutional Review Board (IRB protocol number 827644). All patients provided written informed consent in accordance with local regulatory review. Patient samples were collected with written informed consent and ethics approval under the same IRB protocol. The Data Safety Monitoring Board provided oversight and monitored the safety of the study.

The median age at study entry was 61 years (range: 45–74 years). Among the patients infused with huCART-meso cells, three (33.3%) were reported as male and six (66.7%) as female. All participants were Caucasian. Gender information was based on patient self-report. Patient characteristics are summarized in Table S1.

Cell lines

AsPC-1 (human cell line, female) and HEK293T (human cell line, female) cells were acquired from the American Type Culture Collection (ATCC), which reports cell line sex information. AsPC-1 cells were cultured in DMEM/F12 (1:1) (Gibco, Life Technologies), 20% fetal bovine serum (FBS), and 1% penicillin/streptomycin (Gibco, Life Technologies). HEK293T cells were maintained in RPMI-1640 (Gibco, Life Technologies) supplemented with 10% FBS, 2% HEPES (Gibco), 1% GlutaMAX (Gibco), and 1% penicillin/streptomycin. Authentication of all cell lines was regularly performed by the University of Arizona Genetics Core, and mycoplasma contamination was routinely assessed using the MycoAlert Mycoplasma Detection Kit (Lonza).

Mice

Animal experiments were conducted following protocols approved by the Institutional Animal Care and Use Committee of the University of Pennsylvania. Six-to eight-week-old NOD/scid/IL2rγ−/− (NSG) female mice were obtained from Jackson Laboratories and bred in the vivarium at the University of Pennsylvania under pathogen-free conditions. The mice were housed and maintained in a pathogen-free environment throughout the study. Sex was assigned based on provider information and visual inspection.

Primary human T lymphocytes from healthy donors

Primary T lymphocytes from healthy donors were sourced from the University of Pennsylvania Human Immunology Core, with the approval of the University of Pennsylvania Institutional Review Board (IRB protocol number 700906) All samples were deidentified to comply with HIPAA rules. Participants in the study provided written informed consent, adhering to the principles outlined in the Declaration of Helsinki, the International Conference on Harmonization's Good Clinical Practice guidelines, and the United States Common Rule. The reported gender and age for each sample are as follows: ND539 (male, 39), ND561(male, 27), ND410 (female,

CellPress
OPEN ACCESS

59), ND582 (female, 54), ND602 (male, 40), ND609 (male, 25), ND584 (male, 31), ND528 (male, 31). Gender information was based on donor's self-report.

METHOD DETAILS

Lentiviral vector production

The production of lentiviral vectors was conducted following previously established protocols.[88] In brief, HEK293T cells were transfected with lentiviral CAR and packaging plasmids using Lipofectamine 2000 or Lipofectamine 3000 (Invitrogen) according to the manufacturer's instructions. Lentiviral supernatants were harvested at 24- and 48-h time points post-transfection and concentrated using high-speed ultracentrifugation. The resulting concentrated lentivirus batches were then resuspended in cold media (RPMI 1640 medium supplemented with 10% fetal bovine serum (FBS), 1% L-glutamine, 1% penicillin-streptomycin) to generate lentiviral stocks, which were subsequently stored at −80°C.

Transduction of CAR-redirected human T cells

The huCART-meso is a second-generation CAR comprising a human MSLN-binding single-chain variable fragment (scFv), and CD8α hinge and transmembrane domains fused to 4-1BB and CD3-ζ cytoplasmic signaling domains. CAR T cells were manufactured as previously described.[89] Briefly, primary human $CD8^+$ and $CD4^+$ T cells from healthy donors were mixed at 1:1 ratio and activated at a concentration of 1 x 10^6 cells/ml using Dynabeads CD3/CD28 CTS (Thermo Fisher Scientific) at a 3:1 bead-to-cell ratio. Approximately 24 h later, the T cells were transduced at a multiplicity of infection (MOI) of 3–5. Beads were magnetically removed from the cultures on day 5. T cell cultures were maintained at a concentration of 8 x 10^5 cells/ml. Cell number and volume were monitored daily using a Multisizer 4 Coulter Counter (Beckman Coulter). Transduced T cells were cryopreserved upon reaching the resting state, as determined by cell size.

Flow cytometry and sorting

Fresh metastatic tissue collected by fine-needle aspiration and recurrent tumors from *in vivo* experiments were collected, processed and stained in fresh. Samples were digested in RPMI containing collagenase D (400 Mandl units/mL, Sigma) and DNase I (50 mg/mL, Sigma) for 15 min at 37°C to generate single cell suspensions. 12 μL/mL EDTA 0.5 M, pH 8 was added to stop the enzymatic digestion. Samples were then mechanically disrupted and filtered through a 0.7 mm cell strainer (Corning). Ammonium-Chloride-Potassium (ACK, GIBCO) Lysing Buffer was used for the lysis of red blood cells. Human infiltrating T cells from recurrent mice were enriched by magnetic sorting prior to FACS sort by using the EasySepTM Release Human CD45 Positive Selection Kit for Humanized Mice (STEMCELL Technologies) according to manufacturer's instructions. Single-cell suspensions from processed tumors and *in vitro* cultures were washed in PBS and stained with Fixable Dead Cell Dyes followed by FcR-Block treatment (Fc Receptor Blocking Solution, Biolegend) as per manufacturer's recommendations.

Patient ascites were collected and centrifuged at 500g, at 4C for 20min. Patient's 04 sample was enriched by Ficoll Paque Plus density gradient following manufacturer's protocol.

Viable T cell counts were determined using a trypan blue stain (Invitrogen) and a Countess automated cell counter (Invitrogen). Samples were then stained in fluorescence-activated cell sorting (FACS) buffer, which consisted of PBS (Gibco), 0.5% bovine serum albumin (BSA) (GEMINI), 2 mM EDTA (Invitrogen), and 100 μg/mL DNase (Roche). To calculate absolute cell counts in cell suspensions, CountBrightTM Absolute Counting Beads (ThermoFisher) were used as an internal standard following the manufacturer's instructions.

Antibodies for surface staining are detailed in the key resources table. Surface expression of huCART-meso was assessed using either biotinylated goat anti-human IgG F(ab')2 (Jackson ImmunoResearch, 109-066-006) followed by fluorochrome-conjugated streptavidin (see the key resources table), or an anti-idiotype antibody (provided by Novartis Pharmaceuticals). The anti-idiotype antibody was specifically used for detecting huCART-meso in patient-derived samples.

Live/dead staining was performed using Live/Dead Aqua (Life Technologies) or Zombie NIR (Biolegend) Fixable Viability Kits according to the manufacturer's protocol, followed by cell surface staining for 15 min at 4°C in the dark. Samples were analyzed on an LSRII Fortessa and BD Symphony A5 Flow Cytometers (BD Biosciences) and processed using FlowJo v10 software (FlowJo, LLC). Sorting assays were performed using a FACS Aria Fusion Cytometer (BD Biosciences).

Clinical trial design

This was a single-center, single-arm phase 1 study designed to evaluate the safety and feasibility of both intravenous and local administration of lentivirally transduced huCART-meso cells in patients with histologically confirmed unresectable or metastatic pancreatic adenocarcinoma. The rationale for the phase 1 study was informed by previous CAR T cell trials conducted by our group. Based on prior experience with MSLN-directed CAR T cell therapies, we hypothesized that local delivery of the maximum tolerated dose (MTD) of huCART-meso cells (established by i.v. infusion under NCT03054298, 1-3x10^7 huCART-meso cells/m^2) may reduce the risk to patients by mitigating the potential for off-tumor, on-target toxicities. To further balance toxicity and efficacy, the study permitted repeat i.v. infusions of huCART-meso cells every 21–42 days at the clinical discretion of the physician-investigator after

the initial local dose. We aimed to test if the repeat i.v. infusions would bolster the anti-tumor effect of persistent huCART-meso cells, which could lead to improved clinical outcomes while mitigating risk of toxicities observed at higher i.v. doses.

Eligible patients for the study have histologically confirmed unresectable or metastatic pancreatic adenocarcinoma. Additional enrollment criteria included: (1) failure of at least one prior standard of care chemotherapy for advanced stage disease; (2) measurable disease as defined by RECIST 1.1 criteria; (3) patients $\geq$18 years of age; (4) Eastern Cooperative Oncology Group performance status of 0 or 1; (5) satisfactory organ and bone marrow function; (6) blood coagulation parameters: PT such that internal normalized ration is $\leq$1.5 and a PTT $\leq$1.2 time the upper limit of normal unless the patient is therapeutically anti-coagulated for history of cancer-related thrombosis and has stable coagulation parameters; (7) provides informed written consent; and (8) patients of reproductive potential must agree to use acceptable birth control methods.

All subjects who received the target dose of huCART-meso cells were considered evaluable for response, including progression-free survival and overall survival. All subjects with radiologically confirmed measurable disease (per RECIST 1.1) at baseline were considered evaluable for overall radiologic response.

Clinical Cell manufacture

Enrolled patients underwent apheresis at the Hospital of the University of Pennsylvania Apheresis Center. The manufacture and release testing of huCART-meso cells were performed by the Clinical Cell and Vaccine Production Facility at the University of Pennsylvania, according to Phase 1 IND current Good Clinical Manufacturing Practice guidelines and FACT Common Standards for Cellular Therapies. huCART-meso cells are autologous T cells that have been engineered to express an extracellular single chain antibody with mesothelin specificity and 4-1BB/TCRζ intracellular signaling domains. T cells were enriched from autologous leukapheresis products and activated with anti-CD3/CD28 antibody-coated magnetic beads, followed by transduction with the lentiviral vector containing the huCART-meso transgene. T cells were expanded in culture and washed, de-beaded, and cryopreserved in infusible grade cryomedia prior to product release following confirmation of FDA-specified release criteria for sterility, purity, and identity.

Quantitative PCR analysis of clinical samples

Each amplification reaction contained 200 ng of genomic DNA per time point for peripheral blood and tumor samples. To determine copy number per unit DNA, an eight-point standard curve was generated consisting of between 5 and 10^6 copies of huCART-meso lentivirus plasmid spiked into 200 ng of nontransduced control genomic DNA. The number of copies of plasmid present in the standard curve was verified using digital qPCR with the same primer/probe set and performed on a QuantStudio 3D digital PCR instrument (Life Technologies). Each data point (sample and standard curve) was evaluated in triplicate with a positive cycle threshold value in three out of three replicates with a percentage coefficient of variation <0.95% for all quantifiable values. To control for the quantity of interrogated DNA, a human genomic DNA reference assay was performed using 10 ng of genomic DNA and a primer-probe combination specific for a nontranscribed genomic sequence upstream of the CDKN1A (p21) gene, as previously described.[90] These amplification reactions generated a correction factor to adjust for calculated versus actual DNA input. Copies of transgene per microgram DNA were calculated according to the formula: copies/microgram genomic DNA = copies calculated from huCART-meso standard curve x correction factor/amount of DNA evaluated (ng) x 1000 ng.

Serum cytokine profiling

Serum samples obtained before and after huCART-meso infusion and cryopreserved at −80°C were thawed and analyzed for cytokine measurements using a 31-plex panel (Millipore Sigma) as previously described.[91]

Production of human CRISPR-Engineered CAR-T cells

The design and synthesis of single guide RNA (sgRNA) sequences targeting ID3 and SOX4 were performed according to previously established methods.[26] Gene disruption, T cell activation, transduction, expansion, and knockout validation followed an optimized protocol as described.[92] Briefly, primary T cells were cultured in OPT 7/15 media, which consist of OpTmizer T cell expansion media (Gibco) supplemented with 5 ng/mL of huIL-7 and huIL-15 each (Preprotech). After 24 h, cells were electroporated using the Lonza 4D-Nucleofector Core/X Unit and the P3 Primary Cell 4-D Kit. For Cas9 and sgRNA delivery, RNP complexes were formed by separately incubating 10μg of each sgRNA with the Cas9 nuclease (Aldevron, 10 μg) for 10 min at room temperature (RT). Cells were spun down at 300xg for 5 min and resuspended at a concentration of 5-10x10^6 cells/100μL in the specified buffer (P3 Solution with Supplement). The RNP complex, 100μL of resuspended cells, and 4μL of 100μM IDT Electroporation Enhancer (a non-homologous ssDNA oligonucleotide) were combined and electroporated in a cuvette. Following electroporation, the cells were cultured in OPT 7/15 media at a concentration of 5 x 10^6cells/mL at 37°C and activated 4 to 6h later using anti-CD3/anti-CD28 monoclonal antibody-coated magnetic beads. After 24 h, T cell were lentivirally transduced and expanded as described above.

For each target locus defined by two sgRNA cut sites (spanning 100 and 130 bp for SOX4 and ID3, respectively), PCR and sequencing primers were designed to detect the target loci. LongAmp Taq 2X Master Mix (NEB) was utilized for target sequence amplification following the manufacturer's protocol, and DNA purification was performed using NucleoSpin Gel and PCR Clean-up (Macherey-Nagel). Gene editing efficiency was evaluated by Sanger sequencing as previously described.[26] Synthego's Performance Analysis ICE tool was employed to calculate the editing efficiency. Primer sequences used for KO generation and editing efficiency validation are provided in Table S3.

Mouse experiments

NOD/scid/IL2rγ−/− (NSG) mice were purchased from The Jackson Laboratory and bred and housed in the vivarium at the University of Pennsylvania in pathogen-free conditions. Animal studies were approved by the University of Pennsylvania Institutional Animal Care and Use Committee. Mice were subcutaneously injected with 2×10^6 AsPC-1 cells suspended in 200 μL Matrigel:PBS (1:1) into the right flank. When the mean of tumor volumes reached 250–300 mm^3, mice were treated with 0.5 or 1 x 10^6 huCART-meso cells generated from different healthy donors. Tumor volumes were calculated as $length \times with^2 \div 2$. Tumor growth was weekly assessed by caliper measurement. After primary antitumor response mice were monitored for recurrence. Mice bearing recurrent tumors were sacrificed when reached the maximum size or showed evident signs of disease, and tumors were collected.

Standard immunohistochemistry (IHC) analyses

Recurrent tumors were collected and processed for standard IHC analysis by the Comparative Pathology Core at the School of Veterinary Medicine of the University of Pennsylvania. Formalin-fixed tissues were routinely processed for paraffin embedding, sectioning, and staining. 5-μm-thick paraffin sections were mounted on ProbeOn slides (Thermo Fisher Scientific). The immunostaining procedure was performed using a Leica BOND RXm automated platform in combination with the Bond Polymer Refine Detection Kit (Leica). Rabbit monoclonal primary antibody against human CD45 (CD45-LCA; Cell Signaling Technology, catalog no. 13917) was used at concentrations of 1:300 and incubated on the sections for 45 min at room temperature. A biotin-free polymeric IHC detection system, consisting of horseradish peroxidase–conjugated anti-rabbit immunoglobulin G (IgG), was applied for 25 min at room temperature. Immunoreactivity was visualized using the diaminobenzidine chromogen. CD45 infiltration was quantified using Aperio ImageScope v12.4 (Aperio Technologies, Vista, CA, USA).

Single-cell RNA-seq library preparation

scRNA-seq libraries were generated using a Chromium Single-Cell 3′ v3.1 Library and Gel Bead Kit (10x Genomics) following the manufacturer's protocol. Briefly, for recurrent mouse tumor and chronic antigen stimulation assays, $CD8^+$ T cells were sorted by FACS and washed with ice-cold PBS +0.04% BSA. After washing, 15,000 cells were loaded onto the chromium controller to generate single-cell gel beads in emulsion. For patient samples, approximately 35,000–100,000 $CD3^+$ T cells were sorted by FACS and cells were washed twice with ice-cold PBS +0.04% BSA and spun down at 600g for 5 min. After washing, cells were resuspended in up to 45 μL of ice-cold PBS +0.04% BSA. Five microliters of cell suspension were mixed with 5 μL of trypan blue, and cell numbers were counted via hemacytometer under the microscope. Approximately 10,000–16,000 cells were loaded to create the gel bead in emulsion. Following reverse transcription, gel beads in emulsion were disrupted and barcoded complementary DNA was isolated and amplified. After fragmentation, end repair, and poly A tailing, sample indexes were added and amplified following the manufacturer's protocol. The final libraries were quality control checked and sequenced on an Illumina NextSeq 500. Patient 04 was sequenced with a 75-cycle kit with parameters Read 1: 28, Read 2: 56, Index 1: 8, Index 2: 0. Recurrent mouse tumors and patient 05 were sequenced with a 150-cycle kit with parameters Read 1: 28, Read 2: 91, Index 1: 8, Index 2: 0.

Single-cell RNA-seq analysis

To assess the expression of huCART-meso CAR in the scRNA-seq data, the cellranger reference was reindexed (mkref) by adding a single contig for the 818 bp WPRE sequence (a unique sequence in the CAR plasmid) to the GRCh38 assembly of the human genome (the gene annotation GTF file was appended with CDS and exon entries spanning the entire sequence and gene_id ''CAR-Ligand''). Sequencing data were aligned to the GRCh38 genome with the WPRE sequence and then barcodes and unique molecular identifiers were counted using the Cell Ranger v3.1.0 command cellranger count. See below detailed analyses for each experiment.

Patient and recurrent tumor TILS single cell (Figures 2 and 4)

Data were further analyzed in R (version 4.2.0) using Seurat version 4.3.0.1.[85,86] Briefly, genes that were not detected in at least 3 cells and cells with >10% mitochondrial reads were excluded, as well as cells that express <200 genes or >5000 genes. Data were normalized using NormalizeData. CellCycleScoring was performed using s_genes and g2m_genes. Data were normalized using sctransform V 0.3.5 [87] with assay = RNA, new.assay.name = 'SCT', vst.flavor = "v2", vars.to.regress = S.Score, G2M.Score, percent.mt. RunPCA was performed with npcs = 30. Samples were integrated using Seurat's integration method[86] with the following parameters. SelectIntegrationFeatures (nfeatures = 3000) and FindIntegrationAnchors using "SCT" was run. Next, we used RunUMAP on integrated datasets with "pca" reduction and dims = 1:20. FindClusters was performed with a resolution of 0.4 and UMAPs were generated.

Patient single cell (Figure 2)

Marker genes were determined using the FindAllMarkers function in Seurat using SCTransform normalized expression values where at least 25% of the cells must be expressing the gene with a logfc.threshold = 0.25. Next, ALRA imputation method[93] was performed to reduce the number of technical zeros. ALRA imputed data was used to generate the UMAP feature plot of CAR expression. To isolate CARpos cells, subset function was used with parameter CAR-Ligand>0 using ALRA imputed values. 537 CARpos cells were identified. Next, CARneg cells were randomly downsampled to 537 cells using set.seed equals 12. CARpos and downsampled CARneg Seurat objects were merged using the merge function. After merging, RunALRA was performed on the merged object. Genes differentially expressed between CARpos and CARneg cells were identified using FindMarkers. Imputed values were plotted via violin plot to show expression changes between CARpos and CARneg cells. Z scores were calculated from imputed values for the

30 dysfunction signature genes and pheatmap was used to generate heatmaps with ward.D clustering method using down-sampled data.

T cell subpopulations were defined using canonical markers. In the CD4 population, we detected regulatory T cells (Tregs; FOXP3, IL2RA, IKZF2), naive (SELL, CCR7, LEF1), and effector memory T cells (Tem; IL7R, KLRB1). In the CD8 population, we detected memory T cells (Tmem; CCR7, LEF1, SELL, IL7R, TCF7), effector memory (Tem; IL7R, KLRG1, NKG7), GZMK+ effector memory (GZMK+ Tem; GZMK, NKG7, PRF1, GZMH, CCL5), terminally differentiated Tem (Temra; NKG7, PRF1, GZMH, CCL5), and an NK-like T cell population (NK-like; NCAM1, FCGR3A, GNLY, GZMB, KLRC1, KLRC2). To display changes in T cell subpopulations, the number of cells found within each cluster for each condition was normalized by the total number of cells per condition and expressed as percentages. Cell type composition analysis in single-cell data was implemented using propeller from speckle R package.[84] Briefly, moderated t-tests method was performed on cell type proportion between huCAR-meso+ (CARpos) and endogenous CAR negative T cells (CARneg) replicates for all cell types, excluding the unknown annotated cluster. P-values were reported as statistical significance.

Recurrent tumor TILs single cell (Figure 4)

To isolate CARpos cells, the subset function was used with parameter CAR-Ligand>0. SCTransform normalized expression values were used to make violin plots and UMAP feature plots. Genes differentially expressed between WT and SOX4KO recurrent tumor CARpos TILs were identified using FindMarkers. Wilcoxon Rank-Sum test was used to measure significance and adjusted *p*-values were calculated based on Bonferroni correction to determine the level of significance comparing WT to SOX4KO recurrent tumor TILs and data was plotted via violin plot.

T cell subpopulations were defined using canonical markers. All cell clusters expressed exhaustion markers LAG3, HAVCR2, TOX, TIGIT. Clusters were further classified by NK-like Tex which expressed high levels of NK receptors and CAR T cell exhaustion genes identified in [26] (KLRC1, KLRC2, KLRB1, KLRD1, CD9, TNFRSF18, RGS16, and SRGAP3.) The GZMK+ Tex population was identified as having high expression of GZMK and EOMES and low to no expression of NK receptors and CAR T dysfunction signature genes. To display changes in T cell subpopulations, the number of cells found within each cluster for each condition was normalized by the total number of cells per condition and expressed as percentages. Cell type composition analysis in single-cell data was implemented using propeller from speckle R package.[84] Briefly, moderated t-tests method was performed on cell type proportion between WT and SOX4KO replicates for all cell types. P-values were reported as statistical significance.

QUANTIFICATION AND STATISTICAL ANALYSIS

Statistical analyses were performed using Prism 10.1.2 GraphPad (GraphPad software) are represented by the following $^{****}p < 0.0001$, $^{***}p < 0.001$, $^{**}p < 0.01$, $^{*}p < 0.05$.

Statistical details for all experiments, including the statistical tests used, exact values of n, definitions of n, measures of central tendency, and measures of variability are provided in the figure legends.

For CAR T cell expansion in biopsy samples, statistical analysis was performed using a Wilcoxon matched-pairs signed rank test. For *in vitro* and *in vivo* assays, Normality tests (D'Agostino & Pearson test, Kolmogorov-Smirnov test and Shapiro-Wilk test) were used to assess normality of distribution of the variables. Statistical significance between two groups was determined using two-tailed unpaired Student's test or the equivalent non-parametric Mann-Whitney. For tumor growth data analyses, Mixed effects two-Way ANOVA was used to compare the average tumor growth rates among groups by assessing the significance of the treatment by time interaction term within the timepoints showing linear growths. Statistical significance between multiple groups of two variables was assessed by two-Way ANOVA with post hoc tests.

Kaplan-Meier curves were generated for relapse-free survival (RFS) analyses, defined as the number of days between the date of infusion and the first of the following dates: recurrence, death, end of the experiment (censored). A log rank test for RFS, restricting to WT or DKO subjects was performed.

To identify changes in cell populations from single-cell RNA-seq datasets, significance was evaluated using the moderated t-test using the propeller method, speckle package in R. Data were visualized using the following R packages and functions ggplot2, pheatmap, RColorBrewer, gplots, dplyr, plotly. RFS was analyzed using the survival, SurvMisc, survminer packages in R. See key resources table for versions of R packages utilized in this study.